AD_____

Award Number: DAMD17-99-1-9239

TITLE: Prediction of Pathologic Fracture Risk in Activities of Daily Living and Rehabilitation of Patients With Metastatic Breast Carcinoma of the Pelvis and Femur

PRINCIPAL INVESTIGATOR: Nozomu Inoue, M.D., Ph.D.

CONTRACTING ORGANIZATION: The Johns Hopkins University School of Medicine
Baltimore, Maryland 21205-2196

REPORT DATE: August 2002

TYPE OF REPORT: Final

PREPARED FOR: U.S. Army Medical Research and Materiel Command
Fort Detrick, Maryland 21702-5012

REPORT DOCUMENTATION PAGE

Form Approved
OMB No. 074-0188

1. AGENCY USE ONLY (Leave blank)	2. REPORT DATE	3. REPORT TYPE AND DATES COVERED
	August 2002	Final (15 Jul 99 - 14 Jul 02)

4. TITLE AND SUBTITLE
Prediction of Pathologic Fracture Risk in Activities of Daily Living and Rehabilitation of Patients With Metastatic Breast Carcinoma of the Pelvis and Femur

5. FUNDING NUMBERS
DAMD17-99-1-9239

6. AUTHOR(S)
Nozomu Inoue, M.D., Ph.D.

7. PERFORMING ORGANIZATION NAME(S) AND ADDRESS(ES)
The Johns Hopkins University School of Medicine
Baltimore, Maryland 21205-2196

E-MAIL:
ninoue@jhmi.edu

8. PERFORMING ORGANIZATION REPORT NUMBER

9. SPONSORING / MONITORING AGENCY NAME(S) AND ADDRESS(ES)
U.S. Army Medical Research and Materiel Command
Fort Detrick, Maryland 21702-5012

10. SPONSORING / MONITORING AGENCY REPORT NUMBER

11. SUPPLEMENTARY NOTES
report contains color

12a. DISTRIBUTION / AVAILABILITY STATEMENT
Approved for Public Release; Distribution Unlimited

12b. DISTRIBUTION CODE

13. ABSTRACT *(Maximum 200 Words)*

The purpose of the project was to develop a computer model of the pelvis and proximal femur which could be used to predict pathologic fracture risk and study the effects of pelvic and proximal femoral metastatic bone lesions on the care and management of breast cancer patients. The scope of the research was to construct graphical and quantitative models of the pelvis and proximal femur on a computer workstations including Finite Element Method and Discrete Element Method to study the stress and strain in the pelvis and proximal femur and pressure distribution of the hip joint in the patient with metastatic bone lesions of the breast cancer in the pelvis and proximal femur with interactive capability. This project resulted in the development of a computer model of the hip joint which can be used to predict the pathologic fracture risk and study the effects of metastatic bone lesions on the hip joint. The computer model is user-friendly and interactive, and the critical areas for pathologic fracture during various activities can be demonstrated in three-dimensional graphics and animations. This computer model will aid in planning of non-operative or operative management, rehabilitation regimens, nursing programs, and patient education.

14. SUBJECT TERMS	15. NUMBER OF PAGES
breast cancer, bone metastasis, pathological fracture, virtual reality computer model, rehabilitation, nursing care, quality of life	45
	16. PRICE CODE

17. SECURITY CLASSIFICATION OF REPORT	18. SECURITY CLASSIFICATION OF THIS PAGE	19. SECURITY CLASSIFICATION OF ABSTRACT	20. LIMITATION OF ABSTRACT
Unclassified	Unclassified	Unclassified	Unlimited

Table of Contents

INTRODUCTION

The subject of the project was to develop models to predict the pathologic fracture risk in activities in daily living (ADL), nursing care, and rehabilitation in breast cancer patients with metastatic lesions in the pelvis and proximal femur. The purpose of the project was to develop a computer model of the pelvis and proximal femur which could be used to predict the pathologic fracture risk and study the effects of pelvic and proximal femoral metastatic bone lesions on the care and management of breast cancer patients. The scope of the research was to include the construction of graphical and quantitative models of the pelvis and proximal femur on computer workstations including Finite Element Method (FEM) and Discrete Element Method (DEM) to study the stress/strain in the pelvis and proximal femur and pressure distribution of the hip joint in the patient with metastatic bone lesions of the breast cancer in the pelvis and proximal femur with interactive capability.

BODY

Technical Objectives 1: Computer model construction

Task 1: Establishment of a database for location, size, and distribution of metastatic breast cancer to pelvic and femoral regions.

Seventy-three data sheets of the metastatic breast cancer to the pelvis and femur were created including the radiographic analysis and a database was established (**Appendix 1** and **Table 1**). This database also includes other information beside the location and the size of the metastatic lesion, such as the period from the diagnosis of the breast carcinoma to the diagnosis of the bone lesion, pre-surgical function, histology of the metastatic lesion, type of surgery, and post-surgical function.

The results of the data analysis are shown in **Figures 1- 3**. The results revealed that the incidence of metastatic lesion in the cancellous bone region (epiphysis and epiphysis-metaphysis) was 17.5% of the total femoral lesions, and the locations of the lesions were widely dispersed. The isolated acetabulum lesion was rare (2 cases) in this series. Therefore, it was indicated that the development of an interactive model which allowed individual analysis for each case was more reasonable and valuable than creating several generic models which could be adapted to the individual case. All femoral metastases with tumor size less than 50% of the diaphyseal diameter were considered to have the impending fracture status and did not show actual fractures. The size of the lesion could not be determined in 55.3% of the lesions in the AP radiographs (**Fig. 3A**) and 60% of the lesions in the lateral radiographs (**Fig. 3D**) because of tumor diffuseness and/or permiative expansion of the metastatic lesions.

These results were useful for planning and execution of the following Tasks. This data set would also be useful for evaluation of the QOL of breast carcinoma patients with bone metastasis from multiple points of view in future studies.

Task 2: Development of Multi-Discrete Element Model (DEM) and Finite Element Model (FEM) of pelvic and femoral regions based on the database established in Task 1.

An interactive discrete element model of the hip joint was developed (**Fig. 4**). This model allowed creation of a bone metastasis induced defect at the hip joint surface with any size or location interactively. The features of the model are illustrated in **Figures 5 and 6**. The model demonstrated a remarkable changes in the contact stress distribution in the hip joint when a bone defect existed at the joint surface (**Fig. 6**). Because of the interactive capability, the discrete element model of the hip joint could be performed on an individual basis.

The results of **Task 1** revealed that 52.6% of the femoral metastatic lesions were located in the diaphyseal region. Therefore, a finite element model of the long bone with a bone defect was created, and parametric analyses regarding the size of the defect were performed. A finite element model of a femur diaphysis with a rectangular defect in the posterior cortex was developed to quantify the femur stress distribution and torsional stiffness for defect widths ranging from one-tenth of the femur outer diameter (0.1 OD) to 0.3 OD and defect lengths ranging from 0.5 to 5 OD. Defects with a length of 1 OD or shorter had little

influence on the femur torsional stiffness or the femur shear-stress distribution. The torsional stiffness decreased most dramatically as the defect length increased from 2 to 3 OD, but began to approach an asymptote near 5 OD. Shear flow reversal peaked at the center of the defect for defects longer than 1 OD, and the magnitude of the reversal began to approach an asymptote near 5 OD. For each defect, the largest stresses within the bone developed at the defect corners. The results indicate that the open-section effect decreases the torsional stiffness, and stress concentration effects decrease the torsional strength of a long bone with a longitudinal defect (**Fig. 8**).

Task 3: Mechanical testing using cadaveric specimens of the pelvic region with and without bone defects in the pelvis.

See **Task 4**.

Task 4: Mechanical testing using cadaveric specimens of the femoral region with and without bone defects in the proximal femur.

The purpose of **Task 3** and **Task 4** was to validate the results of the finite element analysis and the discrete element analysis.

Rectangular cortical bone defects were created in the mid-diaphysis (n = 6) to validate the finite element model. Defect length was equal to the outer diameter (1 OD), and the defect width was 0.25 OD. The corners of the defect had a 0.8 mm radius of curvature. Yield torque (measured by an acoustic emission technique) and ultimate torque were evaluated. The results of the finite element model with the same geometry and loading conditions were compared with the experimental results. Fractures were initiated at the corners of the defect under torsional testing, the area where the highest stress/strain was calculated in the finite element model (**Fig. 7**). The mean values of yield torque and ultimate torque obtained from the mechanical tests were 62% and 59% of the intact bones (without defect), respectively, and the torsional strength calculated from the finite element model was 59% of the intact bone. These results indicate that the finite element analysis provided a good prediction of the fracture under this condition.

The results of the finite element analyses shown in **Task 2** indicated that the strength of the bone with a defect was determined by 1) reduction of the bone mass, 2) stress concentration at the defect edge, and 3) open section effect. The bones used for mechanical testing in the current study were normal bones. Therefore, bone tissue surrounding the defect had normal structure. Interestingly, it has been observed that the structural strength of the bone with a defect was increased when the bone mineral in the adjacent area was reduced chemically (unpublished data: personal communication with Dr. David Cohen, Assistant Professor of Orthopaedic Surgery, Johns Hopkins University). This phenomenon may be explained by reduction of stress concentration in the bone adjacent to the defect by decreasing bone mineral and/or material properties. Because the results of **Task 1** demonstrated that 55-60% of the metastatic lesions had diffuse and/or permiative borders, consideration of the changes in the microstructure and bone mineral in the bone adjacent to the metastasis may be necessary to predict the pathologic fracture accurately using the finite element analysis. This would be an important research topic in future projects.

In the original mechanical testing protocol, we planned to apply loading to the central part of the hip joint to validate the discrete element model. However, the highest contact stresses in the hip joint were calculated in various locations in the hip joint during ADL as described in **Task 7**. The experimental study to measure the contact stress distribution under different hip positions is an intensive study and beyond the original protocol. During the period of the current project, quantitative data on the hip joint contact stress distribution during a simulated walking cycle were published (R. von Eisnhart et al. Journal of Orthopaedic Research 17:532-539, 1999). This published study aimed to provide data that could be used to generate and validate computer models of the hip joint. This experimental model used the same loading conditions during gait cycle as those we used in the current study (**Task 6**). Therefore, the data provided by this study were ideal to validate the results of the discrete element model developed in the current project. This study reported a maximum contact stress of 6.4 MPa at heel-strike, 7.7 MPa at mid-stance (2 out of 8 specimens overscaled: $\geq$ 9.75 MPa), 6.4 MPa at heel-off, and 5.4 MPa at toe-off. These

values showed good agreement with our results except the value at mid-stance, which was obtained from the overscaled data (**Figs. 11-13**, **Table 2**). The distribution of the contact pressure distribution illustrated in the study also showed the good agreement with the distribution calculated by the discrete element model (also see **Task 7**). Therefore, the contact stress distribution calculated by the discrete element model was well validated by the experimental study, although the experimental study demonstrated a limitation regarding the range of stress measurement required to detect maximum stress during the activity.

Technical Objectives 2: Establishment of the model to predict fracture risk in activities in daily living, nursing care, and rehabilitation

Task 5: Acquisition of kinematic and force data in Activity in Daily Living (ADL), rehabilitation program, and nursing care.

The purpose of the **Task 5** was preparation of the data for **Task 6**. Please see **Task 6**.

Task 6: Analysis of the loading conditions during the activities studied in Task 5.

The loading conditions during ADL, including walking, climbing stairs, and standing up from a chair, were obtained and incorporated in the discrete element model. In 2001, a data set of the contact forces acting at the hip joint during various activities were publicized through a CD "The CD HIP98" and Internet (www.biomechanik.de) by Georg Bergmann, Biomechanics Laboratory at Free University, Berlin, Germany. The data was directly obtained from four patients with hip implants which had load transducers and a telemetry system. Although the data had been published in several journals earlier, the new data set was designed to share the data among researchers worldwide. This data set is the only available data set obtained from real human patients and has become a standard database for hip joint biomechanical studies. An additional benefit using this data set is that results of a study using this common data set can be shared and compared with other studies which used the same data set as shown in **Task 4**. We incorporated this data set into our model. In our model, changes in magnitudes and directions of the force during the activities were visually demonstrated (**Figs. 9-10**), and these results were used in the analyses in **Task 7**.

Task 7: Analysis of the stability and stress/strain distribution in the metastatic pelvis and proximal femur under the loading conditions predicted in Task 6.

This Task is the practical goal of the entire project. The contact stress distributions in the hip joint during activities was simulated and visualized with the three-dimensional graphics and animations. The contact stress distribution during the activities has been analyzed on the normal hip joint. The examples of the analysis are presented in **Figures 11-13** and **Table 2** (walking), **Figures 14-16** and **Table 3** (climbing stairs), and **Figures 17-19** and **Table 4** (standing from a chair). During walking, the maximum contact stress was 22.4 MPa at mid-stance (**Figs. 11,12**, **Table 2**). The highest contact stress in the acetabulum was in a ventro-superior location. During stair-climbing, the highest contact stress in the acetabulum was in a dorso-superior location. The maximum contact stress was 25.4 MPa in a one-legged position, while the opposite leg was in the swing phase (**Figs. 14,15**, **Table 3**). When standing from a chair the high contact stress in the acetabulum was in a dorso-inferior location. The maximum contact stress was 13.2 MPa when subjects were about to rise from a chair and when the upper body was leaning forward (**Figs. 17,18**, **Table 4**). The maximum contact stress among all activities evaluated was during stair-climbing. In all three activities, the contact areas were smallest when the contact pressure was highest.

Using our model, a bone lesion could be created at any place and with any shape and size on the hip joint interactively using a computer mouse. The remarkable increase in the contact stress adjacent to the lesion is demonstrated in **Figure 6** as an example. The results of the contact stress distribution were demonstrated on the computer screen with three-dimensional graphics almost instantly. The direction of the graphics could be rotated interactively by using the computer mouse so that the results could be seen from the desired viewpoint.

This user-friendly interactive computer model with three-dimensional graphical demonstration of the results would be useful to demonstrate the critical areas for pathologic fracture during various activities of the patient with metastatic breast carcinoma. Operation of the system would be easy even for those who are not familiar with a computer. The model can also be used to study the pathogenesis of osteoarthritis of the hip, preoperative planning of hip osteotomy surgery, assessment of femoral head and acetabulum fractures, and prediction of collapse of the femoral head and evaluation of treatment in avascular necrosis of the femoral head. The simulation and visualization techniques used in the current project have also been adapted to simulate fracture reduction and deformity correction of the long bone fracture under unilateral external fixation (**Appendix 3**).

Task 8: Preparation of publications.

Two manuscripts and four abstracts related to the project were published. A manuscript for the main part of the project is being prepared under the title of "three dimensional dynamic hip contact stress distribution in daily activities."

The project will be presented in "Era of Hope" Department of Defense Breast Cancer Research Program Meeting, Orlando, September 25-28, 2002, in Symposium 7 "Medical/Surgical Considerations" and Poster Session "Clinical Management of Breast Cancer."

KEY RESEARCH ACCOMPLISHMENT

- Establishment of a database of the metastatic breast cancer to pelvis and femur to be used for computer model development.
- Development of a user-friendly interactive computer model to analyze and visualize the critical locations for pathologic fracture in the hip joint during various activities in three-dimensional graphics and animations.

REPORTABLE OUTCOMES

- Manuscripts, abstracts, presentations;

Manuscripts

1) Kim YH, Inoue N, Chao EYS: Kinematic simulation of fracture reduction and bone deformity correction under unilateral external fixation. J Biomech. 2002 Aug;35(8):1047-58. (reprint is attached in **Appendix 3**)

2) Virolainen PH, Inoue N, Nagao M, Frassica FJ, Chao EYS: The effect of doxorubicin, cisplatin, and ifosfamide combination chemotherapy on bone turnover. Anticancer Res. 2002 22(5):1971-5 (Neither a reprint nor a copy of the article is available at the time of the final report submission. A copy of the abstract appearing in PubMed is attached in **Appendix 4**)

Abstracts

1) Rafiee B, Inoue N, Jones K, Deitz L, Aro H, Chao E: Trabecular microstructure in the early stage of cortical defect repair. Transaction of the 46th Annual Meeting of Orthopaedic Research Society. Vol. 25, 216, 2000. (**Appendix 5**)

2) Kim YH, Elias JJ, Inoue N, Chao EYS: Study on external fixator adjustability using simulation and visualization model. Proceedings of 2001 Bioengineering Conference, American Society of Mechanical Engineering (ASME), BED-Vol. 50: 237-238, 2001. (**Appendix 6**)

3) Kim YH, Elias JJ, Inoue N, Chao EYS: Application of virtual interactive musculoskeletal system to bone deformity correction using unilateral external fixator, J. Biomech. 34:S53, 2001. (**Appendix 7**)

4) Inoue N, Rafiee B, Toda I, Tamada T, Suwa F, Aro HT, Chao EYS: Vascular and trabecular microstructures in the early stage of cortical defect repair, J. Biomech. 34:S81-82, 2001. **(Appendix 8)**

Presentations

1) Rafiee B, Inoue N, Jones K, Deitz L, Aro H, Chao E: Trabecular microstructure in the early stage of cortical defect repair. the 46th Annual Meeting of Orthopaedic Research Society, Orlando, March 12-15, 2000.

2) Chao E, Nobuhara K, Elias J, Inoue N, Mattessich S, Nakamura Y: Application of visual, interactive, computational models to orthopaedic surgery. 67th Annual Meeting of American Academy of Orthopaedic Surgeons. Orlando, March 15-19, 2000.

3) Inoue N, Chao EYS. Computer-aided preoperative planning for acetabular osteotomy and total hip arthroplasty. 1st International Symposium and Workshop on Reconstructive Surgery of the Pelvis. Graz, Austria, April 18-20, 2001.

4) Kim YH, Elias JJ, Inoue N, Chao EYS: Study on external fixator adjustability using simulation and visualization model. ASME-BED (American Society of Mechanical Engineering, Bioengineering Division) 2001 Bioengineering Conference, Snowbird, Utah, June 27-July 1, 2001.

5) "Era of Hope" Department of Defense Breast Cancer Research Program Meeting, in Symposium 7 "Medical/Surgical Considerations" and Poster Session "Clinical Management of Breast Cancer," Orlando, September 25-28, 2002.

- Patents and licenses applied for and/or issued;
  None
- Degrees obtained that are supported by this award;
  None
- Development of cell lines, tissue, or serum repositories;
  None
- Informatics such as databases and animal models, etc;
  1) A database for the metastatic breast cancer to pelvic and femoral regions
  2) Interactive Discrete Element Model to calculate contact stress distribution at the surface of the hip joint with any defect (source code is written with C++ language)
- Funding applied for based on work supported by this award;
  None
- Employment or research opportunities applied for and/or received on experiences/training supported by this award.
  1) The Principal Investigator of this award, Nozomu Inoue, M.D., Ph.D., was promoted to Associate Professor of Department of Orthopaedic Surgery, Johns Hopkins University in May, 2000.
  2) The Post-Doctoral fellow, Mehran Armand, Ph.D., funded by this award, was promoted to Senior Professional Staff, Technical Service Department at the Applied Physics Laboratory (APL), Johns Hopkins University in July, 2000
  3) A Post-Doctoral fellow, Yoon Hyuk Kim, Ph.D., funded by this award, was recruited from Korea for the replacement of Dr. Armand in February, 2000. After completion of the project, he returned to Korea and has been recruited as an Associate Professor of Mechanical and Industrial System Engineering, Kyung Hee University, Seoul, South Korea, in August, 2002.

CONCLUSIONS

This study resulted in the development of a computer model of the hip joint which can be used to predict the pathologic fracture risk and study the effects of metastatic bone lesions on the hip joint for the care and management of breast cancer patients. The computer model is user-friendly and interactive, and the critical areas for pathologic fracture during various activities can be demonstrated in three-dimensional graphics and animations. This computer model will aid in planning of non-operative or operative management, rehabilitation regimens, nursing programs, and patient education. In addition, this computer model can be used for non-tumor diseases and trauma such as osteoarthritis, intra-articular fracture of the hip, and avascular necrosis of the femoral head.

BIBLIOGRAPHY

(1) Refereed Journal Articles

1) Elias JJ, Nagao M, Chu YH, Carbone JJ, Lennox DW, Chao EY: Medial cortex strain distribution during noncemented total hip arthroplasty. Clin Orthop 2000 Jan; (370):250-8.

2) Shermak MA, Wong L, Inoue N, Nicol T: Reconstruction of complex cranial wounds with demineralized bone matrix and bilayer artificial skin. J Craniofac Surg 2000 May;11(3):224-31.

3) Jani MM, Sponseller PD, Gearhart JP, Barrance PJ, Genda E, Chao EY: The hip in adults with classic bladder exstrophy: a biomechanical analysis. J Pediatr Orthop 2000 May-Jun;20(3):296-301.

4) Shin DS, Choong PF, Chao EY, Sim FH: Large tumor endoprostheses and extracortical bone-bridging: 28 patients followed 10-20 years. Acta Orthop Scand 2000 Jun;71(3):305-11.

5) Meffert RH, Tis JE, Inoue N, McCarthy EF, Brug E, Chao EY: Primary resective shortening followed by distraction osteogenesis for limb reconstruction: a comparison with simple lengthening. J Orthop Res 2000 Jul;18(4):629-36.

6) Inoue YZ, Frassica FJ, Sim FH, Unni KK, Petersen IA, McLeod RA: Clinicopathologic features and treatment of postirradiation sarcoma of bone and soft tissue. J Surg Oncol 2000 Sep;75(1):42-50.

7) Chu Y, Elias JJ, Duda GN, Frassica FJ, Chao EY: Stress and micromotion in the taper lock joint of a modular segmental bone replacement prosthesis. J Biomech 2000 Sep;33(9):1175-9.

8) Frassica DA, Thurman S, Welsh J: Radiation therapy. Orthop Clin North Am 2000 Oct;31(4):557-66.

9) Pierce MC, Valdevit A, Anderson L, Inoue N, Hauser DL: Biomechanical evaluation of dual-energy X-ray absorptiometry for predicting fracture loads of the infant femur for injury investigation: an in vitro porcine model. J Orthop Trauma 2000 Nov;14(8):571-6.

10) Elias JJ, Frassica FJ, Chao EY: The open section effect in a long bone with a longitudinal defect - a theoretical modeling study. J Biomech 2000 Nov;33(11):1517-22.

11) Frassica FJ, Khanna JA, McCarthy EF: The role of MR imaging in soft tissue tumor evaluation: perspective of the orthopedic oncologist and musculoskeletal pathologist. Magn Reson Imaging Clin N Am 2000 Nov;8(4):915-27.

12) Virolainen P, Inoue N, Young DR, Frassica FJ, Chao EY: Method to remove intramedullary cement prior to mechanical testing in canine segmental replacement model. Biomed Mater Eng 2000;10(2):51-6.

13) Sparks AB, Peterson SN, Bell C, Loftus BJ, Hocking L, Cahill DP, Frassica FJ, Streeten EA, Levine MA, Fraser CM, Adams MD, Broder S, Venter JC, Kinzler KW, Vogelstein B, Ralston SH: Mutation screening of the TNFRSF11A gene encoding receptor activator of NF kappa B (RANK) in familial and sporadic Paget's disease of bone and osteosarcoma. Calcif Tissue Int 2001 Mar;68(3):151-5.

14) Bhimani MA, Wenz JF, Frassica FJ: Pigmented villonodular synovitis: keys to early diagnosis. Clin Orthop 2001 May;(386):197-202.

15) Rose PS, Lietman SA, McCarthy EF, Frassica FJ: Destructive scapular lesion in an infant. Clin Orthop 2001 May;(386):260-2, 264-7.

16) Fung M, Kato S, Barrance PJ, Elias JJ, McFarland EG, Nobuhara K, Chao EY: Scapular and clavicular kinematics during humeral elevation: A study with cadavers. J Shoulder Elbow Surg 2001 May-Jun;10(3):278-85.

17) Genda E, Iwasaki N, Li G, MacWilliams BA, Barrance PJ, Chao EY: Normal hip joint contact pressure distribution in single-leg standing-effect of gender and anatomic parameters. J Biomech 2001 Jul;34(7):895-905.

18) Larsson S, Kim W, Caja VL, Egger EL, Inoue N, Chao EY: Effect of early axial dynamization on tibial bone healing: a study in dogs. Clin Orthop 2001 Jul;388:240-51.

19) Mont MA, Jones LC, Elias JJ, Inoue N, Yoon TR, Chao EY, Hungerford DS : Strut-autografting with and without osteogenic protein-1 : a preliminary study of a canine femoral head defect model. J Bone Joint Surg Am 2001 Jul;83-A(7):1013-22.

20) Lietman SA, Miyamoto S, Brown PR, Inoue N, Reddi AH: Temporal sequence of spontaneous repair of osteochondral defects in the knee joint of rabbit is dependent on geometry of the defect. J Bone Joint Surg Br. 2002 May;84(4):600-6.

21) Mofid MM, Inoue N, Atabey A, Marti G, Chao EYS, Manson PN, Vander Kolk CA: Callus stimulation in distraction osteogenesis. Plast Reconstr Surg. 2002 Apr 15;109(5):1621-9.

22) Gafni RI, McCarthy EF, Hatcher T, Meyers JL, Inoue N, Reddy C, Weise M, Barnes KM, Abad V, Baron J: Recovery from osteoporosis through skeletal growth: Early bone mass acquisition has little effect on adult bone density. FASEB J. 2002 May;16(7):736-8.

23) Tis JE, Meffert RH, Inoue N, McCarthy EF, Machen MS, McHale KA, Chao EYS: The effect of low intensity pulsed ultrasound applied to rabbit tibiae during the consolidation phase of distraction osteogenesis. J Orthop Res 2002 July;20(4):793-800.

24) Virolainen PH, Inoue N, Nagao M, Frassica FJ, Chao EYS: The effect of doxorubicin, cisplatin, and ifosfamide combination chemotherapy on bone turnover. Anticancer Res. 2002 22(5):1971-5.

25) Kim YH, Inoue N, Chao EYS: Kinematic simulation of fracture reduction and bone deformity correction under unilateral external fixation. J Biomech. 2002 Aug;35(8):1047-58.

26) Inoue N, Ohnishi I, Chen DA, Deitz LW, Schwardt JD, Chao EYS: Effect of pulsed electromagnetic fields on osteotomy gap healing in a canine tibial model. J Orthop Res 2002 Oct. (in press)

27) Inoue N, Ikeda K, Aro HT, Frassica FJ, Sim FH, Chao EYS: Biologic tendon fixation to metallic implant augmented with autogenous cancellous bone graft and bone marrow in a canine model. J Orthop Res 2002 Oct. (in press)

28) Cullinane DM, Lietman SA, Inoue N, Deitz LW, Chao EYS: The effect of recombinant human osteogenic protein-1 (bone morphogenetic protein-7) impregnation on allografts in a canine intercalary bone defect. J Orthop Res. 2002 Dec. (in press)

29) Matsuura M., Lounici S, Inoue N, Chao EYS: Can accelerated fatigue provide accurate prediction of external fixator reusability? Clin Orthop (in press)

(2) Abstracts

1) Kim YH, Elias JJ, Inoue N, Chao EYS: Study on external fixator adjustability using simulation and visualization model. Proceeding of 2001 Bioengineering Conference, American Society of Mechanical Engineering (ASME), BED-Vol. 50: 237-238, 2001.

2) Kim YH, Elias JJ, Inoue N, Chao EYS: Application of virtual interactive musculoskeletal system to bone deformity correction using unilateral external fixator, J. Biomech. 34:S53, 2001.

3) Inoue N, Rafiee B, Toda I, Tamada T, Suwa F, Aro HT, Chao EYS: Vascular and trabecular microstructures in the early stage of cortical defect repair, J. Biomech. 34:S81-82, 2001.

4) Chao EYS, Kim YH, Elias JJ, Inoue N, Frassica FJ: Effect of diaphyseal and metaphyseal defect on long bone structural strength: a theoretical study. J. Biomech. 34:S73-74, 2001.

(3) Book Chapters

1) E.Y.S.Chao, N.Inoue, J.J.Elias, F.J.Frassica: Computational biomechanics using image-based models, IN: Handbook of Medical Image Processing (Ed. Frank J., Brody W., Zerhouni E.), pp 29-29, Academic Press, San Diego, 2000.

2) E.Y.S.Chao, N.Inoue, F.J.Frassica, F.H.Sim: Segmental Bone/Joint Replacement Using Guided Tissue Regeneration, IN: Tissue Engineering and Biodegradable Equivalents. (Edited by Lewandrowski, Wise, Trantolo, Gresser, Yaszemski, Altobelli), pp 355-384, Marcel Dekker Inc. New York, 2002.

3) N.Inoue, E.Y.S.Chao: Biomechanics of osteoporotic bone and fractures, IN: Internal Fixation in Osteoporotic Bone (Ed. An Y.Y.), pp 9-21, Thieme Medical, New York, 2002.

4) K.Aflatoon, D.A.Frassica, N.Inoue, F.J.Frassica: Bone fixation in patients with bone tumors, IN: Internal Fixation in Osteoporotic Bone (Ed. An Y.Y.), pp 178-185, Thieme Medical, New York, 2002.

(4) Presentations

1) Cullinane DM, Inoue N, Rafiee B, Meffert RM, Tis JE, Deitz LW, Chao EYS: Dose effect of pulsed electromagnetic fields on osteotomy gap healing augmentation. Int. Soc. of Fracture Repair, Hong Kong, 2000.

2) Inoue N, Cullinane DM, Wu T, Deitz LW, Chao EYS: Effect of pulsed electromagnetic fields on bone cells at a distant site. Int. Soc. of Fracture Repair, Hong Kong, 2000.

3) Cullinane DM, Rafiee B, Lietmen SA, Inoue N, Deitz LW, Matsuura M, Chao EYS: The effect of osteogenic protein-1 impregnated allograft on a canine intercalary bone defect. Trans. 47th Ann. Meeting Orthop. Res. Soc., San Francisco, 2001.

4) Rafiee B, Lietman SA, Inoue N, Deitz L, Matsuura M, Cullinane D, Mahmood F, Chao EYS: Stimulation of bone formation in large canine bone allografts by osteogenic protein-1 with type-I collagen carrier. Trans. 47th Ann.Meeting Orthop. Res. Society, San Francisco, 2001.

5) Inoue N, Chao EYS: Computer-aided preoperative planning for acetabular osteotomy and total hip arthroplasty. 1st International Symposium and Workshop on Reconstructive Surgery of the Pelvis. Graz, Austria, April 18-20, 2001.

6) Kim YH, Elias JJ, Inoue N, Chao EYS: Study on external fixator adjustability using simulation and visualization model.ASME-BED (American Society of Mechanical Engineering, Bioengineering Division) 2001 Bioengineering Conference, Snowbird, Utah, June 27-July 1, 2001.

7) Kim YH, Elias JJ, Inoue N, Chao EYS: Application of virtual interactive musculoskeletal system to bone deformity correction using unilateral external fixator. Biomechanica IV, Davos, Switzerland, September 23-25, 2001, J. Biomech. 34:S53, 2001.

8) Inoue N, Rafiee B, Toda I, Tamada T, Suwa F, Aro HT, Chao EYS: Vascular and trabecular microstructures in the early stage of cortical defect repair. Biomechanica IV, Davos, Switzerland, September 23-25, 2001, J. Biomech. 34:S81-82, 2001.

9) Chao EYS, Kim YH, Elias JJ, Inoue N, Frassica FJ: Effect of diaphyseal and metaphyseal defect on long bone structural strength: a theoretical study. Biomechanica IV, Davos, Switzerland, September 23-25, 2001, J. Biomech. 34:S73-74, 2001.

10) Inoue N, Virolainen P, Ikeda K, Frassica FJ, Chao EYS: Effect of autogenous cortico-cancellous inlay grafting on extracortical bone bridging and ingrowth in experimental segmental bone replacement prosthesis fixation with multidrug chemotherapy. 11th Meeting of International Society of Limb Salvage (ISOLS), Birmingham, United Kingdom, October 10-12, 2001.

11) Lietman SA, Inoue N, Rafiee B, Cullinane DM, Deitz LW, Matsuura M, Chao EYS: Stimulation of bone formation in large canine bone allografts by osteogenic protein-1. 11th Meeting of International Society of Limb Salvage (ISOLS), Birmingham, United Kingdom, October 10-12, 2001.

12) Fukuroku J, Inoue N, Rafiee B, Matsuura M, Tan X, Frassica FJ, Chao EYS: Effect of osteogenic protein-1 on experimental cortical bone bridging and ingrowth over porous-coated segmental replacement prosthesis using allogenic cortical bone onlay grafting. 11th Meeting of International Society of Limb Salvage (ISOLS), Birmingham, United Kingdom, October 10-12, 2001.

13) Lietman SA, Inoue N, Frassica FJ: The partial pelvis replacement for acetabular defect. Annual Meeting of Musculoskeletal Tumor Society (MSTS), Baltimore, May 11-12, 2001.

14) Inoue N, Virolainen P, Ikeda K, Frassica FJ, Chao EYS: Effect of multidrug chemotherapy on extracortical bone bridging and ingrowth in experimental segmental bone replacement prosthesis fixation. Annual Meeting of Musculoskeletal Tumor Society (MSTS), Baltimore, May 11-12, 2001.

15) Fukuroku J, Inoue N, Rafiee B, Matsuura M, Tan X, Frassica FJ, Chao EYS: Effect of osteogenic protain-1 on extracortical bone and ingrowth over porous-coated segmental replacement prosthesis using allogenic cortical bone onlay grafting. Trans. 48th Ann. Meeting Orthop. Res. Soc., Dallas, 2002.

16) Inoue N, Cullinane D, Gordon N, Wu T, Deitz L, Simon B, Chao EYS: Secondary effects of pulsed electromagnetic fields on bone turn over at a distant site. Trans. 48th Ann. Meeting Orthop. Res. Soc., Dallas, 2002.

17) Inoue N, Cullinane D, Rafiee B, Meffert R, Tis J, Deitz L, Schwardt J, Chao EYS: Dose effect of pulsed electromagnetic fields on osteotomy gap healing in a canine model. Trans. 48th Ann. Meeting Orthop. Res. Soc., Dallas, 2002.

18) Kim Y, Inoue N, Elias J, Chao EYS: Kinematic simulation of fracture & bone deformation under external fixation. Trans. 48th Ann. Meeting Orthop. Res. Soc., Dallas, 2002.

19) "Era of Hope" Department of Defense Breast Cancer Research Program Meeting, in Symposium 7 "Medical/Surgical Considerations" and Poster Session "Clinical Management of Breast Cancer," Orlando, September 25-28, 2002.

LIST OF PERSONNEL RECEIVING PAY FROM THE RESEARCH EFFORT

Nozomu Inoue, M.D. Ph.D.: Associate Professor of Orthopaedic Surgery,
Johns Hopkins University
Stephen Mattessich, M.S.: Computer scientist, Department of Orthopaedic Surgery,
Johns Hopkins University
Smain Lounici, M.S.: Bioengineer, Department of Orthopaedic Surgery,
Johns Hopkins University
Mehran Armand, Ph.D.: Post-doctoral fellow, Department of Orthopaedic Surgery,
Johns Hopkins University
Yoon Hyuk Kim, Ph.D.: Post-doctoral fellow, Department of Orthopaedic Surgery,
Johns Hopkins University

Appendix 1

RETROSPECTIVE REVIEW FORM OF METASTATIC BREAST CARCINOMA TO PELVIS AND FEMUR

1. Age of breast carcinoma diagnosis

2. Period from breast carcinoma diagnosis to metastatic bone lesion discovery

3. Period from metastatic bone lesion discovery to fracture

4. Type of fracture:
   1 = impending
   2 = active

5. Period from metastatic bone lesion discovery to diagnosis of bone lesion

6. Single or multiple bone fracture

7. Primary tumor histology

8. Grade of histological malignancy

9. Weight (kg) of the patient at fracture

10. Functional status (prefracture):
    1 = ambulatory without aids
    2 = ambulatory with aids
    3 = mobilized in a wheelchair
    4 = bedridden
    5 = unknown

11. Other coexisting disease

12. Other site of metastasis

13. Preoperative pain status:
    1 = at the lesion of metastasis
    2 = adjacent joint
    3 = other site
    4 = none

14. Condition of the primary lesion:
    1 = completely cured
    2 = suspicious residual tumor
    3 = obvious residual tumor
    4 = untreated
    5 = unknown

<u>Radiographic analysis at first fracture</u>

15. Location in the bone:
    1 = epiphysis
    2 = epiphysis - methaphysis
    3 = methaphysis
    4 = methapysis - diaphysis
    5 = diaphysis, proximal third

6 = diaphysis, mid third
7 = diaphysis, distal third
8 = sacrum
9 = ilium
10 = ischium
11 = pubis
12 = acetablum

16. X-ray report: 1 = soft tissue mass, 2 = no mass

17. Tumor manifestation:
1 = osteoblastic
2 = osteolytic
3 = mixed

Size of bone lesion

18. Dimension AP:
1 = <50% of bone diameter
2 = 50< , <75%
3 = 75< , <100%
4 = unmeasurable

19. Dimension Lateral:
1 = <50% of bone diameter
2 = 50< , <75%
3 = 75< , <100%
4 = unmeasurable

<u>Primary treatment of metastatic bony lesion</u>

20. Radiation:
1= none
2 = before surgery
3 = after surgery
4 = before and after

21. Chemotherapy: 1 = no, 2 = yes

22. Other nonoperative treatment: 1 = no, 2 = yes

Surgical treatment:

23. Period from diagnosis of bone lesion to surgery

24. Type of surgery:
1 = no surgery
2 = no removal of the tumor
3 = biopsy alone
4 = curettage
5 = resection, not curative
6 = resection, curative
7 = amputation
8 = others

25. Tissue diagnosis

26. Materials used at the surgery

Post-surgical rehabilitation

27. Period from the surgery to rehabilitation

28. Period from the surgery to first walk after surgery with any aid

29. Period from the diagnosis of bone lesion to last follow-up or death

30. Status at the last follow-up:
    1 = alive with disease
    2 = alive without disease
    3 = alive unknown disease
    4 = dead with disease
    5 = dead without disease
    6 = dead unknown disease

31. Postoperative pain status:
    1= greatly relieved
    2 = slightly relieved
    3 = no change
    4 = worse
    5 = unknown

32. Best functional status after surgery:
    1 = ambulatory
    2 = ambulatory with aids
    3 = mobilization in a wheelchair
    4 = bedridden
    5 = unknown

33. Failure of treatment:
    1 = no failure
    2 = technical error in surgery
    3 = tumor progression
    4 = inadequate care after surgery
    5 = surgical complication
    6 = others

34. Progression locally: 1 = no, 2 = yes

35. Site of other pathologic fracture

36. Pattern of tumor invasion:
    1 = expensile
    2 = permiative
    3 = others

Appendix 2

Table 1 Retrospective Review of Metastatic Breast Carcinoma to Pelvis and Femur

(All female. Only items related to **Task 1** are shown.)

File #	Age at Dx (yrs)	Period from tumor Dx to bone metastasis discovery (months)	Impending/ Actual fracture I: Impending fracture F:Actual fracture	Functional status (pre-fracture) 1: ambulatory without aids 2: ambulatory with aids 3: mobilized in a wheel-chair 4: bedridden 5: unknown	Location of bone lesion 1: epiphysis 2: epiphysis - methaphysis 3 : methaphysis 4 : methapysis - diaphysis 5: diaphysis, proximal third 6 : diaphysis, mid third 7: diaphysis, distal third 8: sacrum 9: ilium 10: ischium 11: pubis 12: acetablum	Tumor manifestation 1: osteoblastic 2: osteolytic 3: mixed	Tumor size 1: <50% of bone diameter 2: 50<, <75% 3: 75<, <100% 4: unmeasurable		Surgery code 1: no surgery 2: no removal of the tumor 3: biopsy alone 4: curettage 5: resection, not curative 6: resection, curative 7: amputation 8: others
							AP	Lateral	
003	35	155	I	1	4	3	3	3	4
007	54	146	I	1	5	2	3	3	2
008	49	67	I	1	8	-	-	-	1
013	60	52	F	3	6	2	3	3	4
015	50	0	F	1	3	2	3	3	5
017	71	157	F	2	5	2	3	3	4
019	83	20	I	1	4	2	3	3	4
019B	83	20	I	1	8, 9	-	-	-	1
032	63	45	F	2	3	2	4	4	5
033B	75	98	I	2	6	3	4	4	2
033C	75	98	I	2	8	-	-	-	1
034	65	0	I	1	2	-	-	-	1
035	73	0	I	1	5	3	3	3	2
038	60	27	F	2	3	2	2	2	5
044	56	41	I	1	1	-	-	-	1
046	53	36	F	2	4	3	4	4	5
046B	53	36	I	2	8, 11	-	-	-	1
048	49	142	F	2	7	2	4	4	4
049	45	29	F	3	4	3	4	4	5
051	58	47	F	2	3	3	4	4	5
052	61	240	F	1	-	-	-	-	5
073	59	24	I	2	6	3	4	4	2
075	54	27	I	1	2	3	3	3	5
079	65	108	I	2	6	2	3	3	4
084B	47	0	I	1	4	2	3	-	2
086	47	20	F	1	1	2	2	2	5
089	44	135	I	2	6	2	2	2	2
089A	44	135	I	2	8	-	-	-	1
089B	44	144	I	2	6	2	4	4	2
090	45	37	I	1	2	2	3	-	5
090B	45	37	I	2	10, 12	-	-	-	1
092	45	57	I	2	3	2	3	-	5
092B	45	57	I	2	8	-	-	-	1
093	57	72	F	2	3	3	4	4	5
096	39	76	I	2	6	2	3	2	2

File #	Age at Dx (yrs)	Period from tumor Dx to bone metastasis discovery (months)	Impending/ Actual fracture I: Impending fracture F:Actual fracture	Functional status (pre-fracture) 1: ambulatory without aids 2: ambulatory with aids 3: mobilized in a wheel-chair 4: bedridden 5: unknown	Location of bone lesion 1: epiphysis 2: epiphysis - methaphysis 3 : methaphysis 4 : methapysis - diaphysis 5: diaphysis, proximal third 6 : diaphysis, mid third 7: diaphysis, distal third 8: sacrum 9: ilium 10: ischium 11: pubis 12: acetablum	Tumor manifestation 1: osteoblastic 2: osteolytic 3: mixed	Tumor size 1: <50% of bone diameter 2: 50<,<75% 3: 75<,≤100% 4: unmeasurable		Surgery code 1: no surgery 2: no removal of the tumor 3: biopsy alone 4: curettage 5: resection, not curative 6: resection, curative 7: amputation 8: others
							AP	Lateral	
098A	53	39	I	1	5	2	3	3	4
098B	53	51	I	2	3	2	3	3	5
098C	53	51	I	2	8	-	-	-	1
103	37	5	F	1	3	2	4	4	5
109	47	13	I	1	6	2	4	2	4
113A	75	16	F	2	5	2	4	4	4
113B	75	21	F	2	2	2	4	4	5
223C	75	21	I	2	11	-	-	-	1
114A	38	84	F	2	3	2	4	4	5
114B	38	84	I	2	8	-	-	-	1
116A	55	103	F	2	3	2	4	4	5
116B	55	103	F	2	5	3	4	4	4
116C	55	103	I	2	10	-	-	-	1
117	65	24	F	2	5	2	4	4	2
117A	65	24	I	2	8	-	-	-	1
120	68	36	I	2	3	2	3	3	5
121	57	24	I	2	11	-	-	-	1
124B	56	112	I	2	4	2	4	4	2
126	24	2	I	2	2	2	4	4	5
127	53	17	I	2	4	2	3	-	4
132	37	74	I	2	5	2	4	4	2
137	41	55	F	1	3	3	4	4	5
141	50	142	I	2	3	3	4	4	5
142	51	34	I	1	5	2	4	4	4
143	56	89	I	2	6	3	4	4	2
146	45	13	I	2	-	-	-	-	5
150	29	15	F	2	5	2	3	3	4
155A	54	97	F	1	5	3	4	4	4
156	42	60	F	1	3	2	4	4	5
157	44	51	I	1	3	2	3	4	4
160A	43	131	F	1	3	2	4	4	4
161	58	89	F	1	3	2	4	4	5
162	41	58	I	1	5	2	4	4	2
177B	65	58	I	1	6	2	3	3	4
186	63	135	F	1	2	2	4	4	5
200	50	0	I	1	1	1	1	1	1
201	26	168	I	1	2	2	1	-	1
203	55	24	I	1	12	3	4	-	1

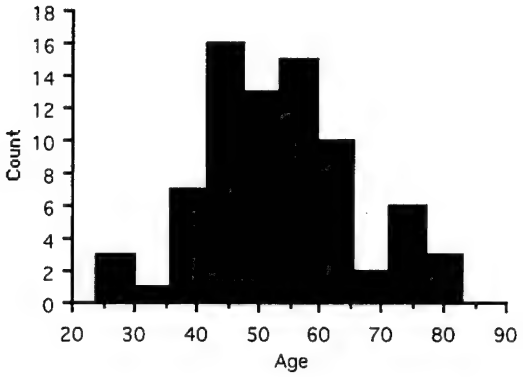

Fig. 1 Histgram of the age of the patients with metastatic breast cartinoma to pelvis and femure.

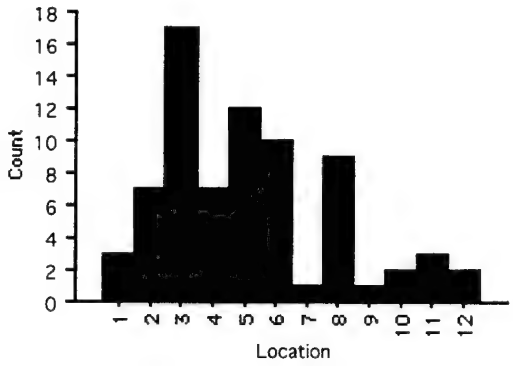

Fig. 2 Histgram of the location of bone lesions. **1**:epiphysis, **2**:epiphysis-methaphysis, **3**:methaphysis, **4**:methapysis-diaphysis, **5**:diaphysis, proximal third, **6**:diaphysis, mid third, **7**:diaphysis, distal third, **8**:sacrum, **9**:ilium, **10**:ischium, **11**:pubis, **12**:acetablum.

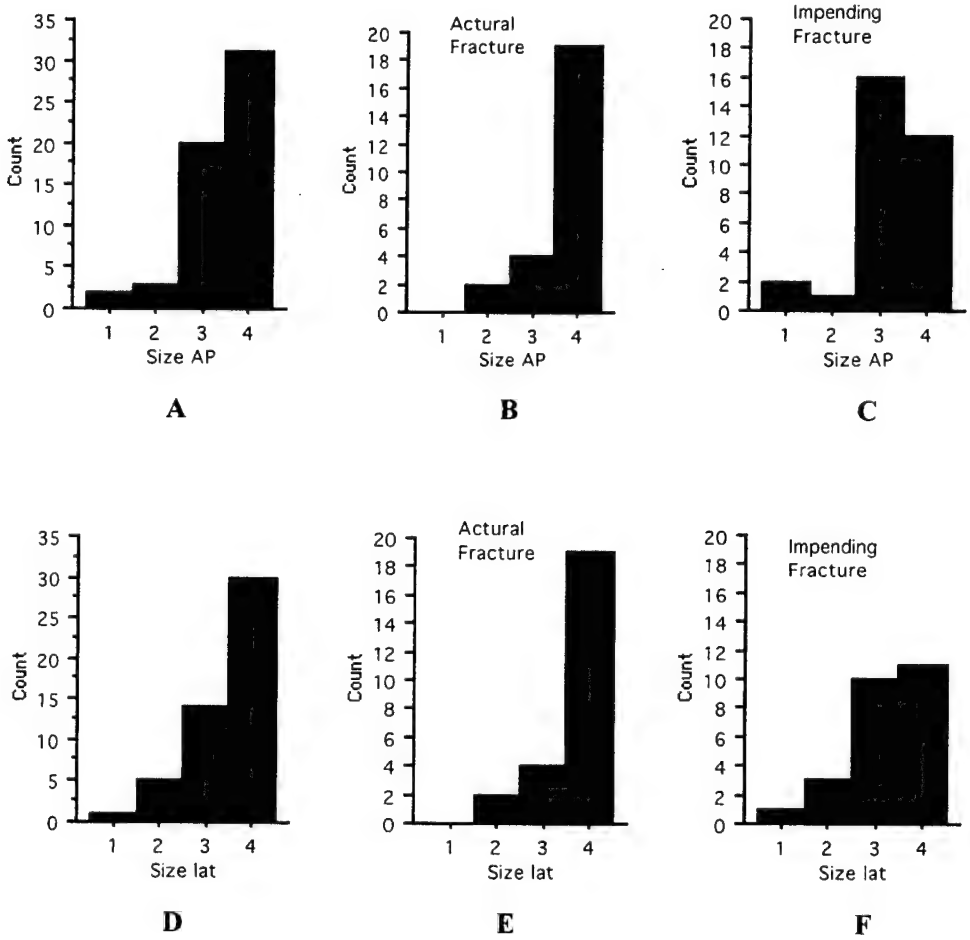

Fig 3A-F Histgrams of the tumor size determined by AP radiograms (**A-C**) and lateral radiograms (**D-F**). **A,D**: Actural fracture and impending fractures. **B,E**: Actual fractures only, **C,F**: Impending fractures only. **1**: <50% of bone diameter. **2**: 50<,<75%. **3**: 75<,<100%. **4**: unmeasurable.

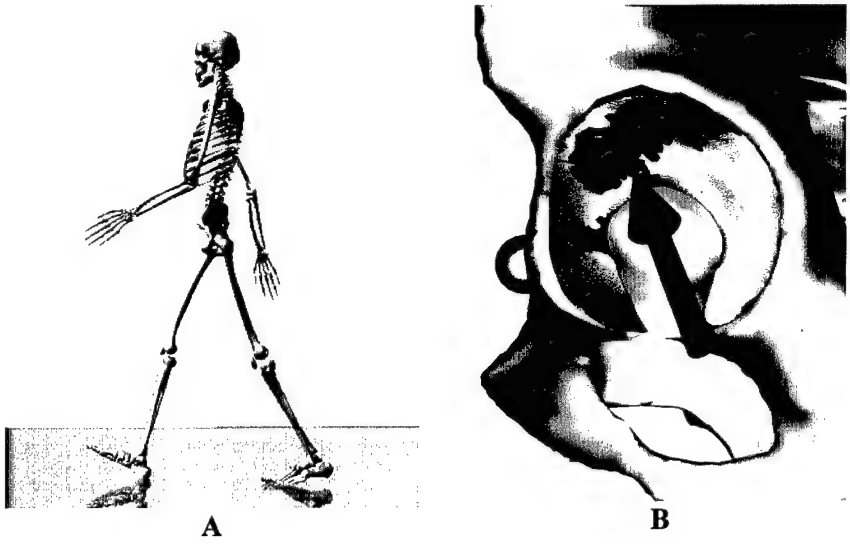

Figs. 4A,B
A: Geometric model of skeleton shown at 55% gait cycle.
B: Acetabular contact stress distribution with the force direction and magnitude represented by a vector. The darkest regions indicate the largest stress.

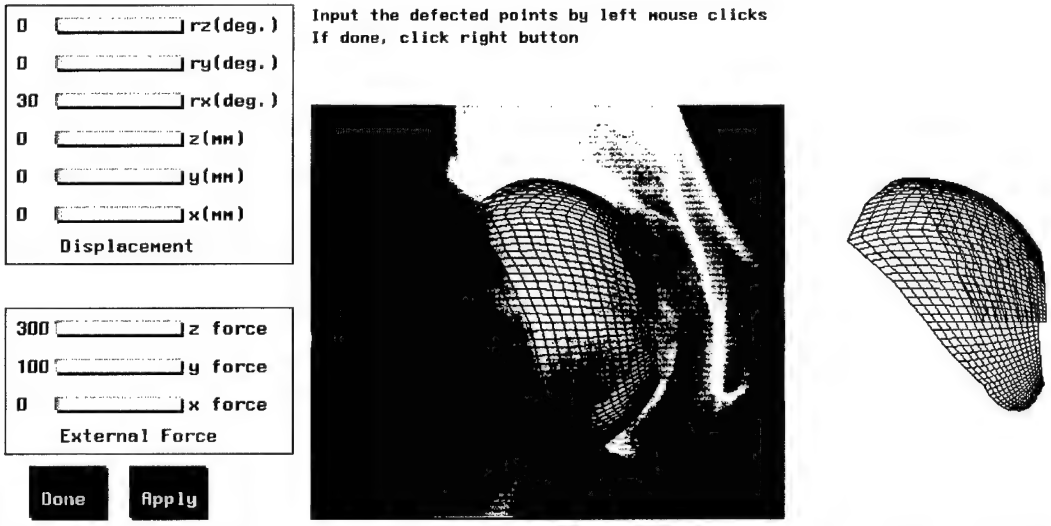

Fig. 5 Interactive discrete element model of the hip joint. Loading conditions and geometry of the acetablum can be input interactively (left and middle). The defect can be generated in any size and location on the surface of the contact surface of the hip joint (left) interactively as well.

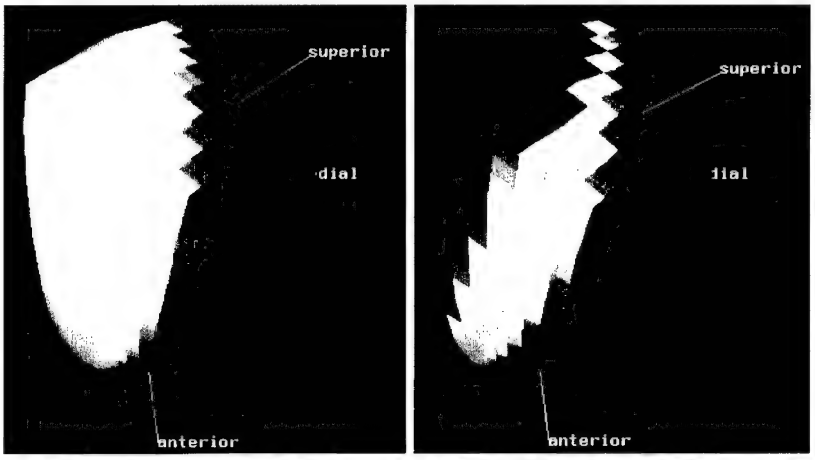

A: Without bone defect **B: With bone defect**

Fig. 6 Contact stress distribution of the hip joint without **(A)** and with **(B)** bone defect calculated by discrete element model. In this example, the contact stress is distributed evenly in the loading area and the peak contact stress is 5.6 MPa **(A)**. Remarkable increase of contact stress is calculated in the adjacent area of the defect (peak contact stress is 10.3 MPa) **(B)**.

Fig. 7 Strain energy density (SED) distribution superimposed over a finite element (FE) model with a defect for a torsional load.

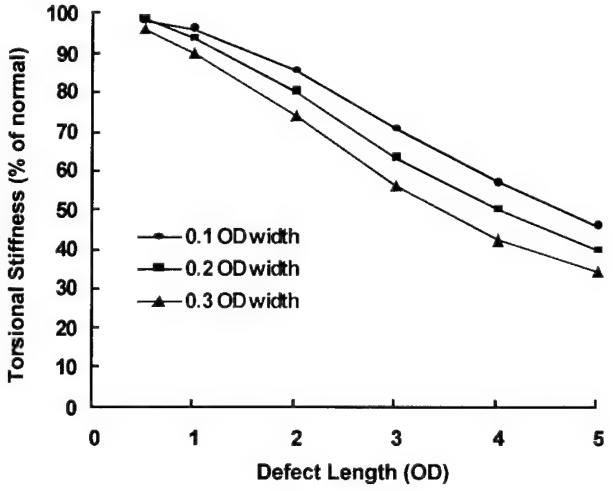

Fig. 8 The torsional stiffness of the femur as a function of defect length for the three defect widths tested. The decrease in torsional stiffness was minimal until the defect length reached 1 OD for all widths. The largest decrease in torsional stiffness with increasing defect length occurred from 2 to 3 OD for each defect width. The torsional stiffness began to taper off beyond a defect length of 3 OD. Similar trends for the increase in shear flow reversal with increasing defect length indicate that the open section effect is the primary influence on the mid-diaphysis torsional stiffness.

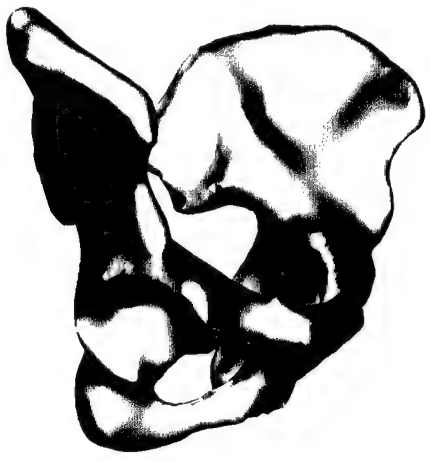

Fig. 9 Three-dimensional pelvic model.

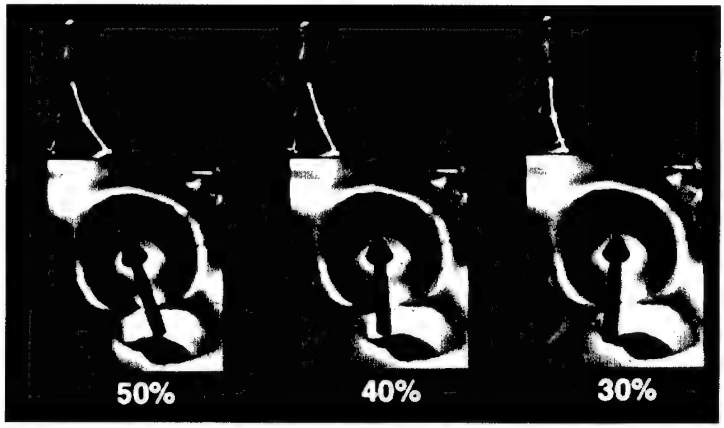

Fig 10 Changes in force direction and magnitude represented by force vectors during normal gait cycle.

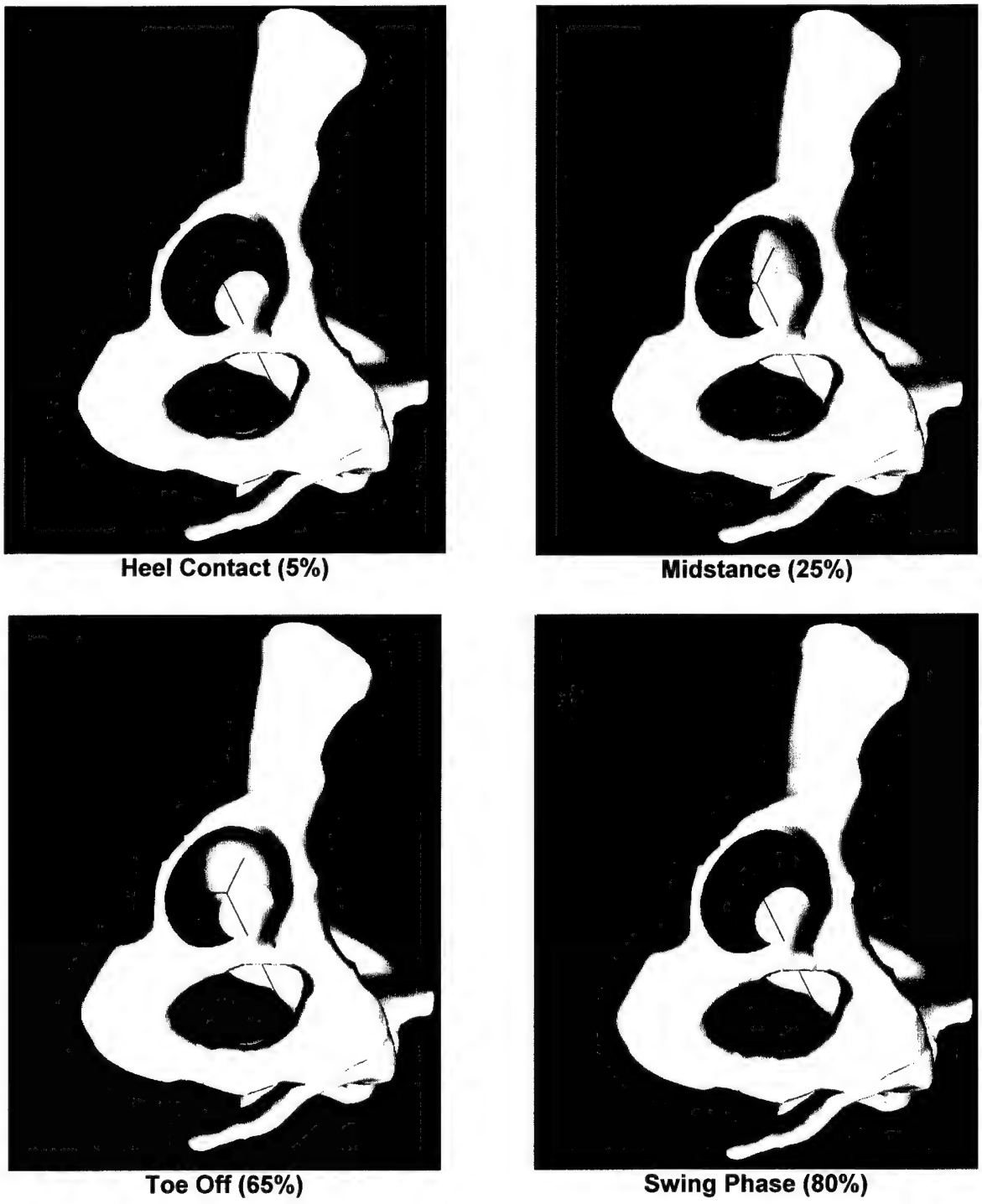

Fig. 11 Contact stress distribution of the acetabulum during walking of four phases: Heel-Contact, Midstance, Toe-Off, and Swing Phase (% of cycle).

Table 2 Joint contact force, contact area, peak contact stress and its location for 12 segments of gait cycle during normal working.

% Cycle	Contact force(x) (%BW)	Contact force(y) (%BW)	Contact force(z) (%BW)	area in contact (cm^2)	Peak contact stress (MPa)	Peak contact stress location (cm)
8.3	22.04	-0.95	68.61	12.81	7.93	(0.86,-1.92,1.34)
16.7	27.89	3.93	100.66	11.61	12.7	(0.5,-2.08,1.28)
25.0	41.6	14.95	173.92	11.37	22.38	(0.5,-2.08,1.28)
33.3	54.68	33.15	227.85	18.96	18.9	(1.64,-0.89,1.65)
41.7	54.19	14.62	201.93	21.2	15.62	(1.52,-0.17,1.97)
50.0	49.73	-3.30	194.13	20.11	14.31	(0.75,-0.069,2.38)
58.3	34.04	2.57	193.79	20.32	10.15	(0.75,-0.069,2.38)
66.7	36.38	1.07	134.57	20.81	5.8	(1.07,-0.065,2.25)
75.0	30.3	-7.04	71.27	18.55	3.26	(1.18,-0.81,2.04)
83.3	16.37	-3.17	36.09	15.38	2.83	(1.27,-1.6,1.43)
91.7	12.34	0.18	25.05	12.61	7.34	(0.16,-1.95,1.54)
100	20.24	-2.19	63.88	24.08	0	(0,0,0)

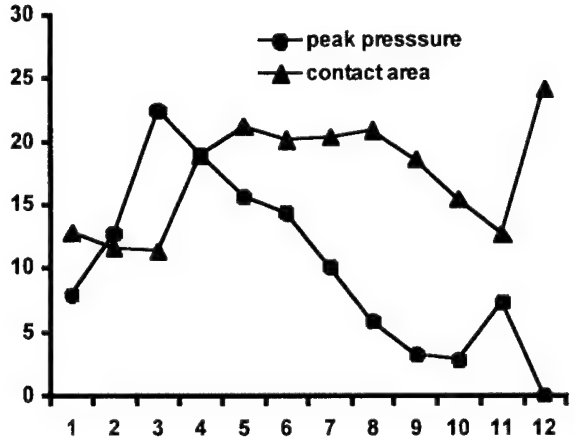

Fig. 12 Contact stresses during normal walking.

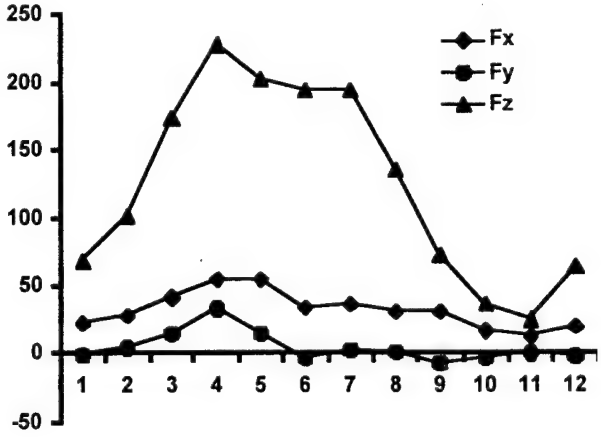

Fig. 13 Contact forces during normal walking.

Fig. 14 Contact stress distribution of the acetabulum during climbing stairs of four phases (% of cycle).

Table 3 Joint contact force, contact area, peak contact stress and its location for 12 segments of motion cycle during climbing stairs.

% Cycle	Contact force(x) (%BW)	Contact force(y) (%BW)	Contact force(z) (%BW)	% area in contact	Peak contact stress (MPa)	Peak contact stress location (cm)
8.3	30.58	8.62	80.4	17.8	9.93	(-0.072,1.96,1.37)
16.7	35.98	13.32	98.89	16.79	19.07	(-0.094,1.53,1.72)
25.0	52.75	38.17	171.07	16.44	25.36	(-1.11,0.82,2.08)
33.3	59.37	60.65	236.32	17.17	18.92	(-0.75,0.21,2.47)
41.7	51.04	40.98	216.82	18.9	15.72	(0.27,-0.22,2.47)
50.0	48.38	10.91	205.03	18.95	17.45	(0.81,-0.48,2.31)
58.3	48.52	4.28	223.65	19.99	10.4	(1.42,-0.53,1.98)
66.7	35.53	-2.59	122.38	22.65	5.19	(1.51,0.058,1.98)
75.0	24.53	-7.06	60.21	23.91	3.62	(1.61,0.8,1.73)
83.3	21.08	-5.33	42.51	23.71	2.88	(1.48,0.85,1.82)
91.7	17.36	0.41	35.24	23.18	3.71	(1.29,0.67,2.03)
100	20.64	1.17	46.8	24.08	0	(0,0,0)

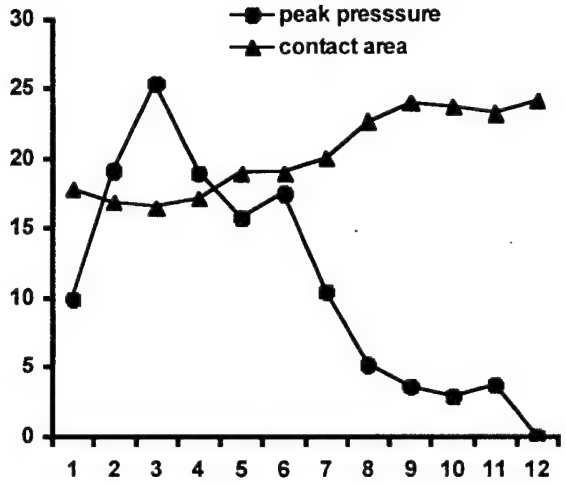

Fig. 15 Contact stresses during climbing stairs.

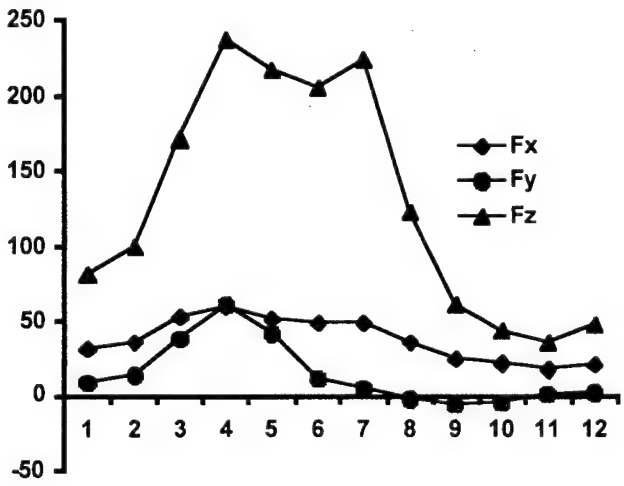

Fig. 16 Contact forces during climbing stairs.

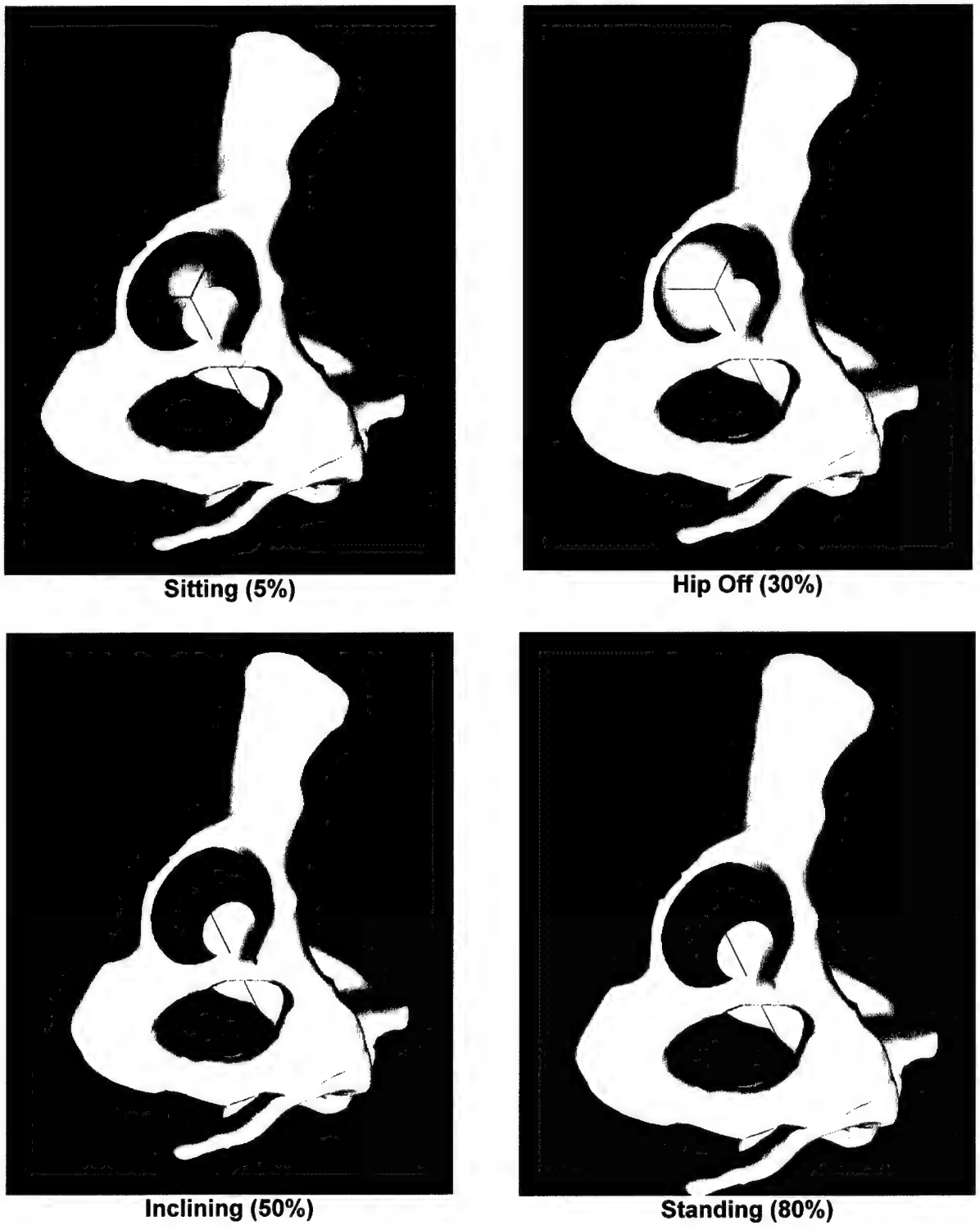

Fig. 17 Contact stress distribution of the acetabulum during standing up from a chair of four phases: Sitting, Hip off, Inclining, Standing (% of cycle).

Table 4 Joint contact force, contact area, peak contact stress and its location for 12 segments of motion cycle during chair up.

% Cycle	Contact force(x) (%BW)	Contact force(y) (%BW)	Contact force(z) (%BW)	% area in contact	Peak contact stress (MPa)	Peak contact stress location (cm)
8.3	6.88	-1.77	22.3	21.96	1.78	(1.84,1.43,0.88)
16.7	7.14	-1.73	21.81	22	1.83	(1.84,1.43,0.88)
25.0	7.48	-1.31	22.24	21.71	2.43	(1.59,1.63,1.01)
33.3	9.02	1.4	31.53	19.43	6.31	(1.01,2.12,0.84)
41.7	21	4.68	83.1	18.86	12.56	(0.91,2.2,0.73)
50.0	43.08	11.3	164.05	21.29	13.16	(1.31,1.8,1.11)
58.3	50	15.41	174.84	23.65	10.31	(1.32,1.31,1.66)
66.7	36.16	15.42	139.6	23.29	7.91	(1.19,0.93,1.98)
75.0	26.93	7.98	108.22	22.12	6.31	(0.95,0.47,2.26)
83.3	21.38	1.71	86.2	21.26	5.87	(0.93,0.2,2.31)
91.7	17.97	-2.1	79.9	21.06	6.37	(0.92,0.068,2.32)
100	18.79	-3.59	85.68	24.08	0	(0,0,0)

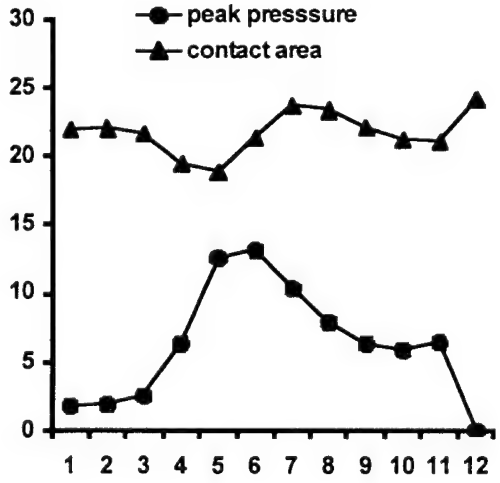

Fig. 18 Contact stresses during standing from a chair.

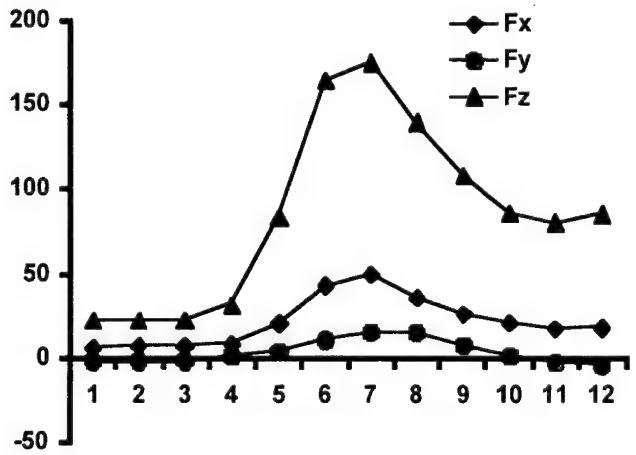

Fig. 19 Contact forces during standing from a chair.

Appendix 3

ELSEVIER

Journal of Biomechanics 35 (2002) 1047–1058

JOURNAL OF BIOMECHANICS

www.elsevier.com/locate/jbiomech
www.JBiomech.com

Kinematic simulation of fracture reduction and bone deformity correction under unilateral external fixation

Yoon Hyuk Kim, Nozomu Inoue, Edmund Y.S. Chao*

Orthopaedic Biomechanics Laboratory, Johns Hopkins University School of Medicine, Ross Research Building, Room 235, 720 Rutland Avenue, Baltimore, MD 21205-2196, USA

Accepted 16 April 2002

Abstract

Combined kinematic analysis and graphic models of two unilateral external fixators are presented to simulate and visualize the correction of bone fracture deformities through systematic adjustments of the fixator joints. The models were developed as rigid linkage systems, and the analysis utilized the 4×4 transformation matrices and the kinematic chain theory to obtain the necessary rotations and translations at each joint of the fixator to correct bone deformities at the fracture site. Three-dimensional malalignments with fracture gaps were simulated to correct the deformities. Due to the redundant pair variables in the fixator joints and other problems in obtaining unique solutions, an optimization technique was used to solve the governing linkage loop equations. For each adjustment solution, the bone correction paths were infinite but a unique and optimal reduction path was obtained by applying corrections to all joints simultaneously and in small increments. When the deformity exceeded a certain range, no admissible solution could be obtained, partially due to the limitation of the unilateral fixator configuration and partially due to the restricted joint rotation and translation in the fixator design. The present models and analysis technique can be used to investigate a fixator's adjustability to correct a 3-D bone deformity at a fracture or lengthening site facilitating patient care planning and medical personnel training.

Keywords: External fixation; Fracture; Bone deformity

1. Introduction

External fixators are commonly used to stabilize long bone segments following fracture or for bone lengthening (Chao and Hein, 1988). After inserting the pins and applying the fixator, adjustment of the position of each segment is often necessary to reduce the fracture and correct any residual deformities. One of the primary goals of external fixator design is allowing adequate adjustability for fracture reduction. Fracture malunion or other bone alignment problems can lead to complications, such as early degenerative disease caused by abnormal joint contact pressures (Cooke et al., 1989; Paley et al., 1990; Chao et al., 1994). For a unilateral external fixator, the ability to adjust rotational and translational deformities is limited (Paley et al., 1990). Previous 2-D studies have quantified malalignment of bone segments based on the alignment of the mechanical axes (Hsu et al., 1990; Paley and Tetsworth, 1992; Heijens et al., 1999), or geometric calculation for rotation deformity only (Matsushita et al., 1998). These approaches could not be used to determine how to adjust complex 3-D deformities with rotational and translational offsets between the bone segments and they did not address how to apply and adjust an external fixator to realign bone segments. Furthermore, the rigid body displacements required to reach the final bone segment reduction at the fracture site are infinite depending upon the sequences of joint adjustment of the fixator selected. A theoretical analysis and graphical model of the bone–fixator system can aid in the selection and optimization of the adjustment required for individual clinical cases.

It has been shown that fracture site or lengthened new bone manipulation, using mechanical means through external fixators, may have beneficial effects on bone healing and remodeling (Egger et al., 1993; Goodship and Kenwright, 1985; Wolf et al., 2001). If favorable

*Corresponding author. Tel.: +1-410-502-6416; fax: +1-410-502-6414.

E-mail address: eyschao@yahoo.com (E.Y.S. Chao).

0021-9290/02/$ - see front matter
PII: S0021-9290(02)00067-2

local mechanical conditions can be reliably and conveniently introduced and maintained using external fixation, skeletal deformity correction and fracture management will be greatly enhanced. These can be readily accomplished through programmed adjustment of fixator joints using well-established biomechanical modeling and analysis techniques.

A combination of an external fixator and a fractured bone can be modeled as a multi-link kinematic linkage system. Such a model can quantify the translations and rotations in the connecting joints of the mechanism necessary to reduce a given fracture or correct a deformity. Combining the kinematic analysis with a graphic model of the bone segments and external fixator allows 3-D visualization of the adjustments required to reduce a fracture. This paper presents models of two external fixators, which can be used to quantify the rotations and translations of each joint of the fixators to correct complex residual fracture deformities in long bones. The model and analysis reported here can also be used to determine the influence of fixator design on the range of adjustability for its mechanical performance.

2. Materials and methods

2.1. Model development

The models of two unilateral external fixators (Dynafix®, EBI, Parsippany, NJ; Orthofix®, Orthofix, Orthofix SRL, Verona, Italy) with different mechanical characteristics and joint designs were used for the present analysis. The Dynafix fixator model is composed of four pins inserted into the bones, two telescoping pin clamps, a central rotary joint and four sets of revolute joints (Fig. 1). The mathematical representation of the motion of each link of the Dynafix fixator and the bone segments was modeled as a kinematic linkage connected by various joints. The revolute joints and the rotary joint were given one rotational degree-of-freedom (DOF), and the telescoping clamps were given one translational DOF which are also defined as a pair variable, which is a unknown independent joint rotation or translation to be determined, in the mathematical analysis. The telescoping clamps were permitted a range of 10 cm of linear adjustment along the long axis of the fixator. The central rotary joint was allowed unlimited rotation and each revolute joint on the telescoping pin clamp was given 60° of rotation in each direction from its neutral position. The Orthofix fixator model is composed of two straight pin clamps with a central body. A telescoping mechanism, which is locked by a compression locking screw, is locked at the central body to provide for 4 cm of axial adjustment. On both ends of the central body, there are two ball-and-socket joints, each allowing 37° of angulation in any direction about the perimeter and an unlimited axial rotation. In both models, all joints began in their neutral positions, with no initial rotation or translation before bone malalignment correction. Other dimensional parameters were

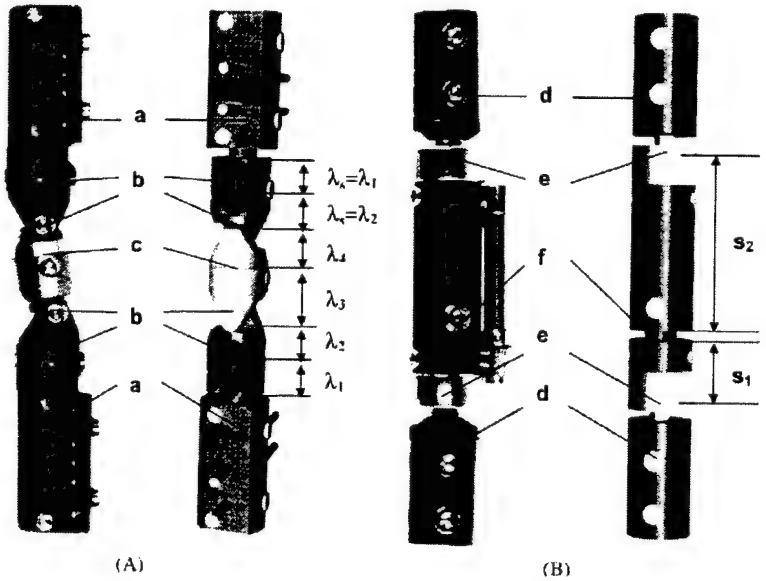

Fig. 1. Comparison of the real (photograph) and the simulated (virtual) models of the two unilateral external fixators. (A) The Dynafix™ fixator (EBI, Medical System Inc., Parsippany, NJ): "a"—the telescoping clamps, "b"—the revolute (serrated hinge) joints, "c"—the central rotary joint. (B) The Orthofix™ fixator (Orthofix, SRL, Verona, Italy): "d" the pin clamps, "e" the ball-and-socket joints, "f" the telescoping central body. Other important dimensional parameters of the fixators have the values: $\lambda_1 = 17$ mm; $\lambda_2 = 25$ mm; $\lambda_3 = 15$ mm; $\lambda_4 = 31$ mm; $\lambda_5 = 25$ mm; $\lambda_6 = 17$ mm; $s_1 = 30$ mm; $s_2 = 90$ mm.

also indicated to facilitate the kinematic simulation analysis (Fig. 1).

The graphic models of the bone–fixator system were developed, using the software Vislab™ (EAI, Ames, IA), to visualize the analysis results of joint rotation and translation required to reduce bone segment malalignment. The tibia model was reconstructed from CT scan data (Visible Human™, National Library of Medicine), while the fixator models were created using the software Vismodel™ (EAI, Ames, IA). All axes of rotation and translation, the local reference coordinate system, the joint degrees-of-freedom, and the fixator and bone dimensions in the graphic model matched those in the real model for the mathematical analysis.

A transverse fracture was simulated at the midshaft of the tibia. The proximal and distal bone segments were modeled as two rigid bodies, with the distal bone segment (D) fixed to the origin of the global coordinate system. The tibia–fixator system construct was modeled as a kinematic linkage system (Fig. 2). Clinically, any malalignment of the proximal segment (P) with respect to the distal segment (D) in terms of angular and translational deformities could be determined from the Biplanar Roentgenogram method using established bone landmarks (Chao and Morrey, 1978). These deformity parameters will be regarded as the known input in the kinematic analysis for fixator adjustment determination.

2.2. kinematic chain analysis

The Orthofix fixator and the tibia with diaphyseal fracture system was modeled as a 4-link and seven DOF spatial linkage not counting the pin/pin-bracket

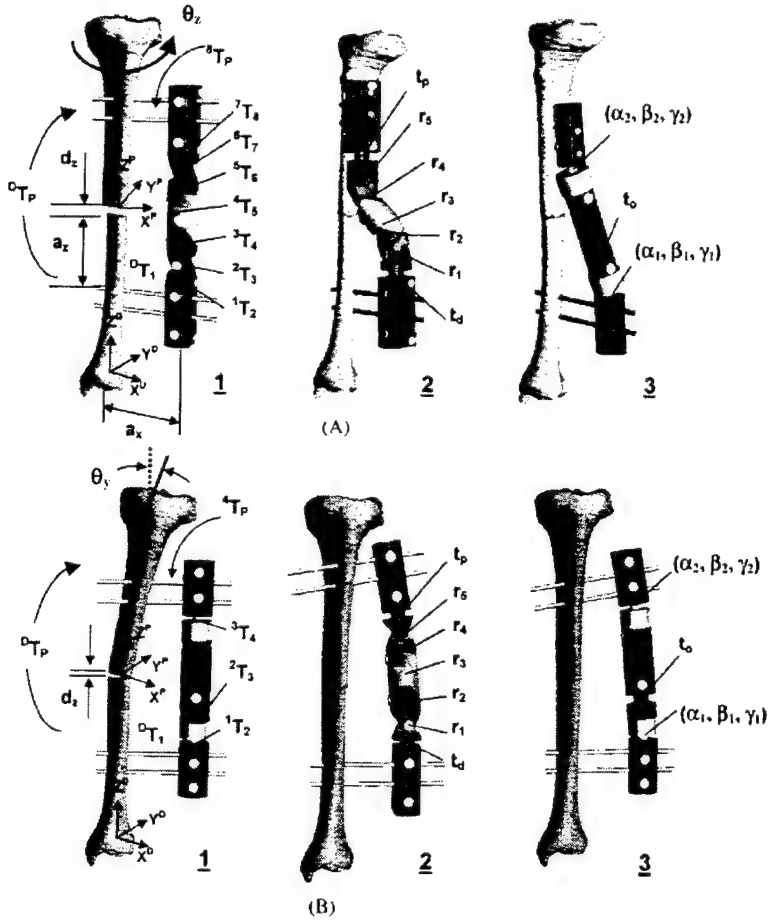

Fig. 2. The tibia–fixator system for the two deformity cases with the transformation matrices. "T" and all the pair variables indicated on the Dynafix and the Orthofix fixators. (A) Bone deformity case 1: $\theta_z = 30^\circ$, $\mathbf{d}_z = 6$ mm. (1) The bone–fixator configuration before correction, the T's are the transformation matrices and $\mathbf{a}_x = 75$ mm, $\mathbf{a}_z = 65$ mm. (2) The unique solution using the Dynafix fixator under the constraint, $\mathbf{t}_d = \mathbf{t}_p$: $\mathbf{t}_p = \mathbf{t}_d = 4.9$ mm; $\mathbf{r}_1 = 14.7^\circ$, $\mathbf{r}_2 = 44.1^\circ$, $\mathbf{r}_3 = -41.9^\circ$, $\mathbf{r}_4 = -42.3^\circ$, $\mathbf{r}_5 = 14.9^\circ$. (3) The unique solution using the Orthofix fixator under the constraint condition, $\gamma_1 = 0$: $\alpha_1 = 17.8^\circ$, $\beta_1 = -4.7^\circ$, $\gamma_1 = 0$, $\alpha_2 = -17.8^\circ$, $\beta_2 = 4.5^\circ$, $\gamma_2 = -28.6^\circ$, $\mathbf{t}_0 = 0.1$ mm. (B) Bone deformity case 2: $\theta_y = 10^\circ$, $\mathbf{d}_z = 3$ mm. (1) The bone–fixator configuration before correction. (2) The unique solution under the constraint, $\mathbf{t}_d = \mathbf{t}_p$: $\mathbf{t}_d = \mathbf{t}_p = 4.8$ mm; $\mathbf{r}_1 = -5^\circ$, $\mathbf{r}_2 = \mathbf{r}_3 = \mathbf{r}_4 = 0$, $\mathbf{r}_5 = -5^\circ$. (3) The unique solution using the Orthofix fixator under the constraint, $\gamma_1 = 0$: $\alpha_1 = -5^\circ$, $\beta_1 = 0$, $\gamma_1 = 0$, $\alpha_2 = -5^\circ$, $\beta_2 = 0$, $\gamma_2 = 0$, $\mathbf{t}_0 = 9.3$ mm.

connection. On the other hand, the Dynafix fixator–bone system is an 8-link and 7-DOF spatial linkage system. According to the well-known Grubler's criteria of linkage movability, both fixator–bone systems had 1 DOF if the fracture was assumed to be completely healed, thus making the linkage chain or movable (Shigley, 1969). The tibial malalignment could have six independent but known rotational and translational deformities that were used to calculate the unknown pair variables of the fixator joints (Chao et al., 1970). This would make the system indeterminate, since there were more pair variables than known bone deformity parameters. In addition, certain pair variables in the current fixator design were redundant (the sliding pair variables on the pin clamps in the Dynafix fixator and the two ball joints on either end of the connecting rod of the Orthofix fixator). To resolve these problems, a least-square minimization method was applied to search for the solution using selected initial estimates for the unknown pair variables. In addition, constraint conditions were introduced to reduce the solution domain of the indeterminate problem.

In order to define the three rotational and three translational malalignments between the two bone segments, a global coordinate fixed to the distal bone segment was described where the X-axis is laterally directed, Y-axis is posteriorly directed, and Z-axis is superiorly directed, respectively (Fig. 2). Similar localized coordinate systems were fixed to the proximal tibial segment and to each of the fixator's movable components. The rotational sequences in the rigid link of the fixator–bone system followed the Bryant Angle convention which used the $X-Y'-Z''$ rotational sequence (Nikravesh, 1988). The prime and double prime symbols denoted the intermediate axes on the moving link. The sign convention of the three rotational deformities was defined by the right-hand rule.

The mathematical expression for the homogeneous transformation matrix using the Bryant Eulerian angle convention (Chao et al., 1970: McCarthy, 1986) is given as Eq. (1)

$$ {}^{D}\mathbf{T}_{P} = \begin{bmatrix} C\theta_y C\theta_z & -C\theta_y S\theta_z & S\theta_y & d_x \\ C\theta_x S\theta_z + S\theta_x S\theta_y C\theta_z & C\theta_x C\theta_z - S\theta_x S\theta_y S\theta_z & -S\theta_x C\theta_y & d_y \\ S\theta_x S\theta_z - C\theta_x S\theta_y C\theta_z & S\theta_x C\theta_z + C\theta_x S\theta_y S\theta_z & C\theta_x C\theta_y & d_z \\ 0 & 0 & 0 & 1 \end{bmatrix}, \tag{1} $$

where θ_x, θ_y and θ_z are the first, the second and the third rotations about the X, Y' and Z'' axes, respectively, d_x, d_y and d_z are three components of the translational vector, and C and S denote Cosine and Sine, respectively.

The relative position and the rotation of the "$i+1$" link with respect to the previous "i" link, is described using the 4×4 homogeneous transformation matrix, (${}^{i}\mathbf{T}_{i+1}$). In the transformation matrix shown in Eq. (1), a revolute joint has one rotational pair variable and a prismatic joint has one translational pair variable. In the case of a ball-and-socket joint, there are three rotational pair variables, whereas the bone fracture site can have total of six displacement variables, three in rotation and three in translation.

2.3. Kinematic loop equations for the Dynafix fixator

In the mathematical analysis of the kinematic chain involving the Dynafix fixator and the tibia, ${}^{D}\mathbf{T}_{P}$ is the transformation matrix from the proximal tibial segment to the distal segment which can also be expressed by the matrix or loop equation:

$$ {}^{D}\mathbf{T}_{P} = {}^{D}\mathbf{T}_{1} \cdot {}^{1}\mathbf{T}_{2} \cdot {}^{2}\mathbf{T}_{3} \cdot {}^{3}\mathbf{T}_{4} \cdot {}^{4}\mathbf{T}_{5} \cdot {}^{5}\mathbf{T}_{6} \cdot {}^{6}\mathbf{T}_{7} \cdot {}^{7}\mathbf{T}_{8} \cdot {}^{8}\mathbf{T}_{P}. \tag{2} $$

${}^{D}\mathbf{T}_{1}$ and ${}^{8}\mathbf{T}_{P}$ represent the rigid body translations of the local coordinate system from the telescoping pin clamp to the bone end at the fracture site (Fig. 2). The matrices, ${}^{2}\mathbf{T}_{3}$, ${}^{3}\mathbf{T}_{4}$, ${}^{5}\mathbf{T}_{6}$ and ${}^{6}\mathbf{T}_{7}$ are pure rotations at the revolute joints, ${}^{4}\mathbf{T}_{5}$ represents the axial rotation at the central rotary joint on the fixator body, and ${}^{1}\mathbf{T}_{2}$ and ${}^{7}\mathbf{T}_{8}$ are for the two prismatic joints. Unknown variables in the transformation matrices can be determined by solving the matrix Eq. (2) based on the known malalignment parameters at the fracture site (${}^{D}\mathbf{T}_{P}$). To facilitate computational convenience, the constant orthogonal matrices ${}^{D}\mathbf{T}_{1}$ and ${}^{8}\mathbf{T}_{P}$ were reduced and the transformation matrix, ${}^{D}\mathbf{T}_{P}$, was adjusted accordingly and represented by ${}^{D}\mathbf{T}_{P}^{*}$. The resultant matrix on the right-hand side of Eq. (2) was defined by ${}^{1}\mathbf{T}_{8}^{*}$ which contains all unknown pair variables of the Dynafix fixator, and Eq. (2) can be reduced to eight nonlinear equations including the seven unknown pair variables, $\mathbf{r}_1$, $\mathbf{r}_2$, $\mathbf{r}_3$, $\mathbf{r}_4$, $\mathbf{r}_5$, $\mathbf{t}_p$ and $\mathbf{t}_d$, as follows:

$$ \begin{aligned} &{}^{D}\mathbf{T}_{P}^{*}(1,1) = {}^{1}\mathbf{T}_{8}^{*}(1,1), \quad {}^{D}\mathbf{T}_{P}^{*}(1,2) = {}^{1}\mathbf{T}_{8}^{*}(1,2), \\ &{}^{D}\mathbf{T}_{P}^{*}(1,3) = {}^{1}\mathbf{T}_{8}^{*}(1,3), \quad {}^{D}\mathbf{T}_{P}^{*}(3,3) = {}^{1}\mathbf{T}_{8}^{*}(3,3), \\ &{}^{D}\mathbf{T}_{P}^{*}(1,4) = {}^{1}\mathbf{T}_{8}^{*}(1,4), \quad {}^{D}\mathbf{T}_{P}^{*}(2,4) = {}^{1}\mathbf{T}_{8}^{*}(2,4), \\ &{}^{D}\mathbf{T}_{P}^{*}(3,4) = {}^{1}\mathbf{T}_{8}^{*}(3,4), \quad {}^{D}\mathbf{T}_{P}^{*}(2,3) = {}^{1}\mathbf{T}_{8}^{*}(2,3), \end{aligned} \tag{3} $$

where, $\mathbf{r}_1$, $\mathbf{r}_2$, $\mathbf{r}_3$, $\mathbf{r}_4$ and $\mathbf{r}_5$ are the revolute pair variables, and $\mathbf{t}_p$ and $\mathbf{t}_d$ are two translational prismatic pair variables, respectively (Fig. 2). The numbers in the

parenthesis indicate the matrix component location for the row and column, respectively. Since there are eight equations with only seven unknown variables, this is an over-determined system (more equations than the unknown variables). However, this over-determinacy is mainly due to geometric constraints, which cannot be derived easily due to non-linear terms in the displacement equations. By using the same optimization method with additional constraint conditions, unique solution can be obtained. The detailed expressions for the elements of the resultant matrix, ${}^{1}\mathbf{T}_{8}^{*}$, are given in the appendix.

2.4. Kinematic loop equations for the Orthofix fixator

In the Orthofix model, assuming that the pin clamp, pins and the tibial bone segment are one rigid link, the transformation from the distal to proximal bone segment can be expressed as

$$ {}^{D}\mathbf{T}_{P} = {}^{D}\mathbf{T}_{1} \cdot {}^{1}\mathbf{T}_{2} \cdot {}^{2}\mathbf{T}_{3} \cdot {}^{3}\mathbf{T}_{4} \cdot {}^{4}\mathbf{T}_{P}, \tag{4} $$

where ${}^{D}\mathbf{T}_{1}$ and ${}^{4}\mathbf{T}_{P}$ represent rigid body translations of the local coordinate system from the telescoping pin clamp to the bone end at the fracture site, ${}^{1}\mathbf{T}_{2}$ and ${}^{3}\mathbf{T}_{4}$ are the rotations of two ball-and-socket joints, and ${}^{2}\mathbf{T}_{3}$ is the translation of the central body.

Similar to the Dynafix case, the constant matrices ${}^{D}\mathbf{T}_{1}$ and ${}^{4}\mathbf{T}_{P}$ were reduced and ${}^{D}\mathbf{T}_{P}$ was redefined as ${}^{D}\mathbf{T}_{P}^{*}$. The resultant matrix on the right-hand side of Eq. (4) became ${}^{1}\mathbf{T}_{4}^{*}$. The resulting eight nonlinear equations were then selected to solve the seven unknown pair variables, α_1, β_1, γ_1, α_2, β_2, γ_2 and $\mathbf{t}_0$, as follows:

$$ \begin{aligned} &{}^{D}\mathbf{T}_{P}^{*}(1,1) = {}^{1}\mathbf{T}_{4}^{*}(1,1), \quad {}^{D}\mathbf{T}_{P}^{*}(1,2) = {}^{1}\mathbf{T}_{4}^{*}(1,2), \\ &{}^{D}\mathbf{T}_{P}^{*}(1,3) = {}^{1}\mathbf{T}_{4}^{*}(1,3), \quad {}^{D}\mathbf{T}_{P}^{*}(3,3) = {}^{1}\mathbf{T}_{4}^{*}(3,3), \\ &{}^{D}\mathbf{T}_{P}^{*}(1,4) = {}^{1}\mathbf{T}_{8}^{*}(1,4), \quad {}^{D}\mathbf{T}_{P}^{*}(2,4) = {}^{1}\mathbf{T}_{4}^{*}(2,4), \\ &{}^{D}\mathbf{T}_{P}^{*}(3,4) = {}^{1}\mathbf{T}_{4}^{*}(3,4), \quad {}^{D}\mathbf{T}_{P}^{*}(2,3) = {}^{1}\mathbf{T}_{4}^{*}(2,3), \end{aligned} \tag{5} $$

where $(\alpha_1, \beta_1, \gamma_1)$ and $(\alpha_2, \beta_2, \gamma_2)$ are the rotational pair variables of the two ball-and-socket joints, ${}^{1}\mathbf{T}_{2}$ and ${}^{3}\mathbf{T}_{4}$. $\mathbf{t}_0$ represents the prismatic pair variable in ${}^{2}\mathbf{T}_{3}$. The detailed expressions for the right-hand sides of Eq. (5) are given in the appendix. If a different Eulerian angle definition of the ball-and-socket joint was chosen, the final form of Eq. (5) could have been different. The resulting over-determined system was solved by the same optimization method described before.

2.5. Solution of the indeterminate kinematic linkage loop equations

Based on the previous spatial linkage movability analysis, both Dynafix and Orthofix systems have 1-DOF, which are movable but could provide non-unique solutions to the same fracture deformity assumed. The resulting loop equations are eight but there are only seven pair variables to be determined. In addition, the number of independent parameters to define the bone deformity is six while the number of pair variables is seven for both fixator systems. This situation created another indeterminacy condition to be resolved in the kinematic loop equations. Furthermore, certain pair variables in the present fixator system may not be independent but their constraint relationships are difficult to derive in closed-form. Finally, the kinematic loop equations are non-linear and contain trigonometric terms that could also produce non-unique solutions. All of these conditions lead to a large solution domain for the present problem.

To reduce the solution domain, two approaches were adopted. One approach was to apply an optimization algorithm to search for the solution of the loop equations using different initial estimates of the pair variable values (Chao et al., 1970). The other approach was to introduce a constraint condition to reduce redundant pair variables in the optimization algorithms applied. In so doing, not only could the solution domain be reduced, but also the rate of convergence in the optimal search scheme would be improved. The following constraint conditions were utilized in the solution process.

2.6. Dynafix fixator

$$ \mathbf{f}(\mathbf{t}_d, \mathbf{t}_p) = 0 \ (\mathbf{t}_d \text{ and } \mathbf{t}_p \text{ are related}), \tag{6} $$

$$ \theta_l < \mathbf{r}_i < \theta_u \ (\text{based on fixator design}), \tag{7} $$

where $\mathbf{f}$ is an intrinsic function, and θ_l and θ_u are the lower and upper bounds of the revolute pair variable $\mathbf{r}_i$.

2.7. Orthofix fixator

$$ \mathbf{g}(\gamma_1, \alpha_2, \beta_2, \gamma_2) = 0 \ (\text{the two ball joints are related}), \tag{8} $$

where $\mathbf{g}$ is an intrinsic function while other constraints similar to that expressed in Eq. (7) were also applied for the Orthofix fixator.

These systems of over-determinate non-linear equations were then solved using the nonlinear least-square optimization method (MATLAB™, Mathworks, MA) with and without the constraint conditions (Chao et al., 1970). In the optimization process, the convergence tolerance of the objective function (summation of the squares of the error terms) was set at 1.e-7. When there were no constraint conditions imposed, multiple solutions were attempted under different initial estimates of the pair variables.

2.8. Graphic animation of fixator adjustment path

Since rigid body finite displacement is sequence dependent, all admissible paths leading to the final fracture malalignment correction should be examined visually. This was profound using a graphic model and simulation tool through animation. Such capability was particularly useful in studying non-unique solutions for the same deformity corrections. When the fixator joint adjustment amount became small, the path dependency condition could be eliminated, providing a unique solution path for the bone during the deformity reduction. To verify the theoretical solution through inspection, the fixator joints were adjusted from end to end either simultaneously or sequentially using small increments. The resulting adjustment paths were examined visually using the graphic model of the system and the kinematic animation of the reduction time history.

To validate the computational results and to examine the adjustment path, two example cases were simulated. In the first example, a rotational malalignment of 30° around the bone long axis with a 6 mm fracture gap between the bone ends was studied. In the second example, a 10° valgus deformity with a 3 mm gap along the long axis of the tibia was investigated (Fig. 2). In these malalignment cases, both fixators were used to demonstrate their capability and options to reduce the bone segments at the fracture site. When multiple solutions for the same deformity were obtained, all solutions and their adjustment sequences, including the use of small and simultaneous joint correction increments, were visually examined for their validity, as well as to observe excessive movement at the fracture site for possible soft tissue distraction or bony interference (collision) during the reduction process.

3. Results

3.1. Unique solution

For the case involving 30° rotational malalignment and a 6 mm fracture gap under the constraint condition of $\mathbf{t}_p = \mathbf{t}_d$, a unique solution for correcting the deformity was obtained for the Dynafix fixator ($\mathbf{r}_1 = 14.7°$, $\mathbf{r}_2 = 44.1°$, $\mathbf{r}_3 = -41.9°$, $\mathbf{r}_4 = -42.3°$, $\mathbf{r}_5 = 14.9°$, $\mathbf{t}_d = \mathbf{t}_p = 4.9$ mm) (Table 1). Other constraint conditions were used but none was effective in producing a unique solution for this deformity case. When the constraint condition $\mathbf{t}_p + \mathbf{t}_d = \mathbf{k}$ ($\mathbf{k}$ is a constant) was applied, multiple solutions were obtained but they were all related to different combinations of the redundant pair variables, $\mathbf{t}_p$ and $\mathbf{t}_d$. In the Orthofix fixator, a unique solution was obtained under the constraint condition of $\gamma_1 = 0$ ($\alpha_1 = 17.8°$, $\beta_1 = -4.7°$, $\gamma_1 = 0.0°$, $\alpha_2 = -17.8°$, $\beta_2 = 4.5°$, $\gamma_2 = -28.6°$, $\mathbf{t}_0 = 0.1$ mm) (Table 2). In the optimization process, the number of iterations was about 2000 in order to get 1.e-7 of the objective function convergence rate. For both fixators the convergence rates were consistent, regardless of the initial estimates for the pair variables. The upper and lower bounds imposed on the fixator revolute joints improved the solution convergence and avoided redundant solutions due to the trigonometric relations.

For the other bone malalignment case with a 10° valgus angulation and a 3 mm gap, the deformity was corrected by a unique correction combination of ($\mathbf{r}_1 = -5°$, $\mathbf{r}_5 = -5°$, $\mathbf{t}_p = \mathbf{t}_d = 4.8$ mm) under the same constraint condition of $\mathbf{t}_p = \mathbf{t}_d$ for the Dynafix fixator. In the Orthofix fixator, the unique solution ($\alpha_1 = -5°$, $\beta_1 = 0°$, $\gamma_1 = 0°$, $\alpha_2 = -5°$, $\beta_2 = 0°$, $\gamma_2 = 0°$, $\mathbf{t}_0 = 9.3$ mm) could be obtained under the same constraint condition of $\gamma_1 = 0$ used in the first example case. Same as before, additional constraints were applied for all revolute pair variables to eliminate possible redundant solutions due to the non-linear algebraic equations involving trigonometric terms. These solutions were unique for both fixators regardless of their initial estimates of the pair variables in the optimization process. Using the simulation models and the graphical animation of the results as a guide, these analytical solutions were verified through visual inspection.

3.2. Non-unique solutions

The main cause of producing non-unique solutions in the fixator–bone systems studied here for bone malalignment adjustment was due to the redundant pair variables in each fixator. Without using any constraint relationships, non-unique solutions were obtained based on different initial estimates for the pair variables for both fixators for the first deformity example case (Tables 1 and 2). Reviewing these results, it was quite clear that certain intrinsic relationships existed among the redundant pair variables for both fixators ($\mathbf{t}_p$ and $\mathbf{t}_d$ for the Dynafix fixator; γ_1, α_2, β_2, and γ_2 for the Orthofix fixator), although the closed-forms of these functional relationships were not established. None of the other pair variable values changed significantly among all solutions. Each of the solution options leads to successful bone alignment correction although the final fixator configurations were different (Fig. 3).

3.3. Optimal bone reduction path

In any solution, the possible reduction paths which the bone segments take to correct the fracture site deformity would be infinite depending on the adjustment sequence options of the fixator joints selected. Since infinitesimal rotations are path independent, unique and non-unique solutions for the fixator joint adjustments were able to produce the same bone

Table 1
Unique and non-unique solutions for the DYNAFIX unilateral external fixator under the fracture malalignment of axial rotation of θ_z (axial rotation) = 30°, $\mathbf{d}_z$ (fracture gap distance) = 6 mm

	Fixator pair variables						
	r_1	r_2	r_3	r_4	r_5	t_d	t_p
Unique solution[a]	14.7	44.1	−41.9	−42.3	14.9	4.9	4.9
Initial estimates	0	0	0	0	0	0	0
Non-unique solution 1	14.3	43.5	−41.1	−41.4	14.4	−4.3	15.5
Initial estimates	0	0	0	0	0	10	0
Non-unique solution 2	13.5	42.2	−40.0	−39.3	13.8	−9.1	20.2
Initial Estimates	0	0	0	0	0	20	0
Non-unique solution 3	13.7	42.5	−40.5	−40.0	14.0	−13.3	24.5
Initial Estimates	0	0	0	0	0	0	10
Non-unique solution 4	14.8	44.3	−41.8	−42.6	14.9	0.4	10.8
Initial Estimates	0	0	0	0	0	0	20
Non-unique solution 5	15.4	45.0	−42.8	−44.1	15.5	5.5	5.6

[a] Using the constraint condition of $\mathbf{t}_d = \mathbf{t}_p$.

Table 2
Unique and non-unique solutions for the ORTHOFIX unilateral external fixator under the fracture malalignment of θ_z (axial rotation) = 30°, $\mathbf{d}_z$ (fracture gap distance) = 6 mm

	Fixator pair variables						
	α_1	β_1	γ_1	t_0	α_2	β_2	γ_2
Unique solution[a]	17.8	−4.7	0.0	0.1	−17.8	4.5	−28.6
Initial estimates	0	0	0	0	0	0	0
Non-unique solution 1	17.8	−4.7	−14.0	0.1	−18.3	0.1	−15.2
Initial estimates	0	0	20	0	0	0	0
Non-unique solution 2	17.8	−4.7	−4.2	0.1	−18.1	3.2	−24.6
Initial estimates	0	0	40	0	0	0	0
Non-unique solution 3	17.8	−4.7	5.1	0.1	−17.4	6.0	−33.4
Initial estimates	0	0	60	0	0	0	0
Non-unique solution 4	17.8	−4.7	13.8	0.1	−16.3	8.5	−41.8
Initial estimates	0	0	80	0	0	0	0
Non-unique solution 5	17.8	−4.7	21.8	0.1	−15.0	10.7	−49.6

[a] Using the constraint condition of $\gamma_1 = 0$.

segment reduction path for the given bone deformity. Using the unique solution and some of the non-unique solutions listed in Tables 1 and 2, bone reduction path was also achieved for both fixators on the same bone deformity case when the pair variable values were divided into 100 increments and adjusted simultaneously (Fig. 4). Although the final configurations of the fixators were very different, the bone reduction paths were identical regardless of the correction solution options or the fixator used. In addition, during this unique bone reduction path, there was no excessive soft tissue distraction or bone end collision. Therefore, by changing all joints simultaneously in small corrections, the bone seemed to take on an optimal path with no bone end collisions or excessive soft tissue disruptions.

3.4. Conditions with no solution

In the unilateral external fixator design, with the restricted parallel pin arrangement on the pin clamps and the adjustable joints located on one side of the long bone, the adjustable range for bone segment malalignment was limited. This limitation was further affected by fixator joint design and the initial placement of the device on the bone. For example, when the fixator was placed in its neutral orientation, it was not able to correct any bone angulation away from the fixator body without being able to slide the bone segment along the pin-group. Another no-solution condition was found in which the axial rotation of the bone segments was more than 57° without any other malalignment involved. When these conditions were combined, the no-solution domain became significantly larger for both fixators studied. Finally, as shown previously, many correction paths in all solutions would produce bone end interference or excessive soft tissue disruption, which should be excluded from the admissible solution domain based on biological considerations as evidenced by graphic simulation and visualization of the bone end movement involved.

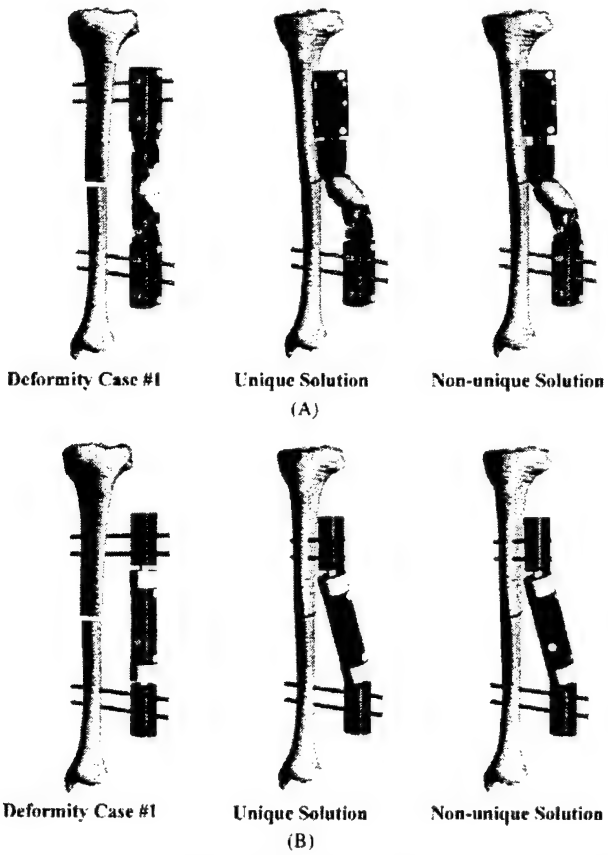

Fig. 3. Comparison of fixator configurations between the unique solution and non-unique (only one was selected) solutions for bone deformity case 1. The differences among these solutions were mainly in the values for the redundant pair variables as demonstrated by the graphic presentations. (A) The Dynafix fixator: among all solutions, $t_d + t_p \cong$ constant (Table 1). (B) The Orthofix fixator: among all solutions, the difference was only in the amount of fixator body rotation about its long axis but such rotation will affect all rotation components of the two ball-and-socket joints (Table 2).

4. Discussion

External fixators are often used for polytrauma cases in emergency environment where adequate imaging equipment is not always available to fully reduce the fracture. Therefore, subsequent adjustment of the fracture ends is often required. Unfortunately, the relationship between fixator adjustment and bone alignment has rarely been investigated. Most of previous studies dealt with description of bone deformities, but to the authors' knowledge there was no prior report in the literature which provided simulation models for the bone and fixator system and analysis techniques to determine the fixator adjustment requirements for 3-D fracture deformity correction. The models, analysis technique, and data reported herewith can provide useful information for the medical personnel who use external fixators in the management of long bone fractures and for device manufacturers to assess their products' efficacy in adjustability, modify their current fixators, or develop new devices.

The results of the current analysis showed that the combination of rotation and translation in bone fracture deformity could be reduced by adjusting a combination of the fixator's joints at certain magnitudes. Without the simulation model and the analysis techniques, such complex reduction pattern could only be determined through trial and error under certain imaging guidance. To reduce difficult fracture deformities, the body of the fixator must be adjusted with all its joints involved in a coordinated manner. Aside from the advantages of providing alignment planning, these models and the analysis software are valuable tools for determining the adjustment limitations of the fixator related to its design, bone malalignment involved, and the clinical application configuration in individual patient. This type of analysis can also provide the application guidelines for a desirable fracture site biomechanical environment to enhance fracture union or bone maturation after lengthening.

Angular deformity in long bone may result from a fracture malunion or caused by metabolic bone diseases

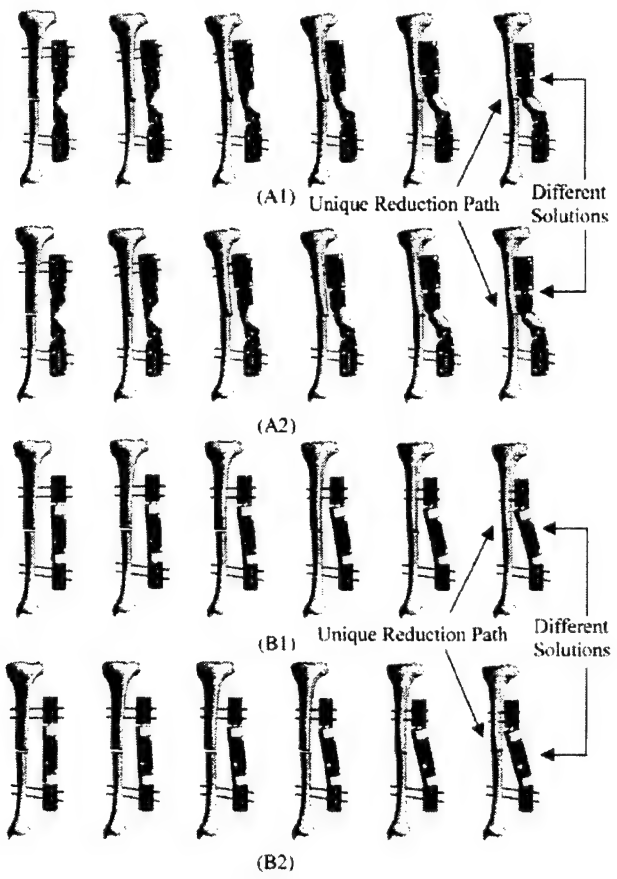

Fig. 4. Sequential graphic visualization of bone–fixator adjustment history for deformity case 1 under different correction solutions. Regardless of the solution or the fixator selected, all bone reduction paths were identical when all pair variables were adjusted simultaneously in small increments. The unique adjustment path for the bone segments seemed optimal since there was no bony collision and the fracture end displacement was minimal during reduction. (A1) Dynafix unique solution; (A2) Dynafix non-unique solutions (only one selected); (B1) Orthofix unique solution; (B2) Orthofix non-unique solutions (only one selected).

or congenital malformation (Paley et al., 1990). The latter types of malalignment often involve pediatric orthopaedic patients and they are often treated by osteotomy (Kanel and Price, 1995). The present model and analysis techniques can be used to plan the placement and subsequent adjustment through external fixation for either one-step correction or gradual distraction after osteotomy. Sequential extension during bone lengthening can cause unexpected bone angulation which can be effectively prevented or corrected through application planning. These are only some of the relevant applications of the simulation models and analysis introduced in this paper.

The two fixators studied produced non-unique adjustment solutions for the two deformity cases in spite of the optimization method used. Such non-unique solution conditions were mainly caused by the redundant pair variables in the fixator joint design. This non-uniqueness problem was easily handled by introducing constraint conditions. However, if the fixator linkage had possessed excessive degrees-of-freedom, additional non-unique solutions may occur and they should be reduced by introducing more constraint conditions. Therefore, external fixators capable of providing bone malalignment adjustment must be evaluated individually using a similar model and analysis technique as presented here.

It is well known that rigid body finite displacement is sequence dependent. In the bone-fixator system, when the adjustment sequence changes, it will produce a different deformity reduction path although the magnitudes of the adjustment for each joint are the same. In addition, finite rotations are not additive even when the well-known Bryant angle convention is used. Therefore, a path-independent or rotation-additive angular measurement system would be important especially when the external fixator is not in its neutral position before the bone malalignment correction takes place. The well-known gyroscopic system (Chao et al., 1980) or the anatomic knee joint system (Grood and Suntay, 1981) would be ideal for the present application. Under such a system, the joint rotational axes are always defined to

facilitate fixator adjustment. The fixator joint may need design modifications to avoid the ball-and-socket configuration and take advantage of this unique rotational axis definition. This feature should be considered for possible manual or motorized adjustment in the next generation of external fixators.

Given a bone fracture malalignment or an osteotomy correction for skeletal deformity, there must be an optimal adjustment strategy for the fixator joints among all correction paths. Since infinitesimal rotation of a rigid body is sequence independent, simultaneous or sequential adjustments with small increments for the fixator joints can be implemented without the concern of which joint needs to be adjusted first. This adjustment solution is able to provide a smooth and efficient reduction path without excessive soft tissue distraction or bone end interference. The graphic animation of the bone end displacement trajectory under small adjustment increment resembles the screw rotation and translation in small steps of one bone segment with respect to the other in order to achieve perfect alignment. Such adjustment strategy would probably be similar to what an orthopaedic surgeon will do to manually reduce the deformity under image guidance. In the future extension of the present analysis software, development of optimal adjustment path for any malalignment must be incorporated using different constraining conditions according to specific clinical application requirements.

The unilateral external fixator has a limited adjustability (Paley and Tetsworth, 1992). This paper only introduced a few simple deformity cases that could be corrected by the two types of unilateral fixators investigated. There are many other situations such as varying fixator design and application configuration, which would make certain bone end malalignments irreducible without taking the fixator off from the bone. When the deformity exceeds a certain range, no admissible solution could be obtained partially due to the limitation of the unilateral configuration and partially due to the restricted range of adjustment inherent to the fixator design. As a result, physicians and nurses trained to use this type of device in patient management must have a thorough knowledge on its adjustment limitation when planning an application. If necessary, certain minimal fracture reduction needs to be achieved before fixator application. In addition, it would be desirable for the manufacturers to establish an information database concerning the biomechanical performance of their devices that should include both the adjustability and stiffness characteristics. Such information can be readily generated using the graphic models and the analysis technique presented in this paper. Finally, the graphic models and the simulation technology offer a unique capability to visualize the intermediate positions of the bone ends and the fixator components during the malalignment reduction path. These are useful tools for personnel training and patient education concerning the biomechanical properties of different fixators and their pitfalls in different application modalities.

Acknowledgements

This study was supported in part by the Orthopaedic Research & Education Foundation (OREF) under the Bristol-Myers Center of Excellence Grant, by the US Army Medical Research and Material Command (USAMRMC) and a gift from EBI Medical Systems Inc.

Appendix. A: Transformation matrix component (row no., column no.) in the loop equations.

A.1. Dynafix

$$^{D}\mathbf{T}^{*}_{P}(1,1) = \cos(\theta_y)\cdot\cos(\theta_z)$$

$$\begin{aligned}^{1}\mathbf{T}^{*}_{8}(1,1) = {} & (\cos(\mathbf{r}_1)\cdot\cos(\mathbf{r}_3)\\ & - \sin(\mathbf{r}_1)\cdot\sin(\mathbf{r}_2)\cdot\sin(\mathbf{r}_3))\cdot\cos(\mathbf{r}_5)\\ & + (-(-\cos(\mathbf{r}_1)\cdot\sin(\mathbf{r}_3)\\ & - \sin(\mathbf{r}_1)\cdot\sin(\mathbf{r}_2)\cdot\cos(\mathbf{r}_3))\cdot\sin(\mathbf{r}_4)\\ & - \sin(\mathbf{r}_1)\cdot\cos(\mathbf{r}_2)\cdot\cos(\mathbf{r}_4))\cdot\sin(\mathbf{r}_5)\end{aligned}$$

$$^{D}\mathbf{T}^{*}_{P}(1,2) = -\cos(\theta_y)\cdot\sin(\theta_z)$$

$$\begin{aligned}^{1}\mathbf{T}^{*}_{8}(1,2) = {} & (-\cos(\mathbf{r}_1)\cdot\sin(\mathbf{r}_3) - \sin(\mathbf{r}_1)\\ & \cdot\sin(\mathbf{r}_2)\cdot\cos(\mathbf{r}_3))\cdot\cos(\mathbf{r}_4)\\ & - \sin(\mathbf{r}_1)\cdot\cos(\mathbf{r}_2)\cdot\sin(\mathbf{r}_4)\end{aligned}$$

$$^{D}\mathbf{T}^{*}_{P}(1,3) = \sin(\theta_y)$$

$$\begin{aligned}^{1}\mathbf{T}^{*}_{8}(1,3) = {} & -(\cos(\mathbf{r}_1)\cdot\cos(\mathbf{r}_3)\\ & - \sin(\mathbf{r}_1)\cdot\sin(\mathbf{r}_2)\cdot\sin(\mathbf{r}_3))\cdot\sin(\mathbf{r}_5)\\ & + (-(-\cos(\mathbf{r}_1)\cdot\sin(\mathbf{r}_3)\\ & - \sin(\mathbf{r}_1)\cdot\sin(\mathbf{r}_2)\cdot\cos(\mathbf{r}3))\cdot\sin(\mathbf{r}_4)\\ & - \sin(\mathbf{r}_1)\cdot\cos(\mathbf{r}_2)\cdot\cos(\mathbf{r}_4))\cdot\cos(\mathbf{r}_5)\end{aligned}$$

$$^{D}\mathbf{T}^{*}_{P}(1,4) = \mathbf{d}_x$$

$$\begin{aligned}^{1}\mathbf{T}^{*}_{8}(1,4) = {} & (-(\cos(\mathbf{r}_1)\cdot\cos(\mathbf{r}_3) - \sin(\mathbf{r}_1)\cdot\sin(\mathbf{r}_2)\cdot\sin(\mathbf{r}_3))\\ & \cdot\sin(\mathbf{r}_5) + (-(-\cos(\mathbf{r}_1)\cdot\sin(\mathbf{r}_3)\\ & - \sin(\mathbf{r}_1)\cdot\sin(\mathbf{r}_2)\cdot\cos(\mathbf{r}_3))\cdot\sin(\mathbf{r}_4)\\ & - \sin(\mathbf{r}_1)\cdot\cos(\mathbf{r}_2)\cdot\cos(\mathbf{r}_4))\cdot\cos(\mathbf{r}_5))\cdot(\lambda_6+\mathrm{t_p})\\ & - \lambda_5\cdot(-\cos(\mathbf{r}_1)\cdot\sin(\mathbf{r}_3) - \sin(\mathbf{r}_1)\cdot\sin(\mathbf{r}_2)\\ & \cdot\cos(\mathbf{r}_3))\cdot\sin(\mathbf{r}_4) - \lambda_5\cdot\sin(\mathbf{r}_1)\cdot\cos(\mathbf{r}_2)\cdot\cos(\mathbf{r}_4)\\ & - (\lambda_3+\lambda_4)\cdot\sin(\mathbf{r}_1)\cdot\cos(\mathbf{r}_2) - \lambda_2\cdot\sin(\mathbf{r}_1)\end{aligned}$$

$$^{D}\mathbf{T}^{*}_{p}(2,3) = -\sin(\theta_x)\cdot\cos(\theta_y)$$

$$\begin{aligned}^{1}\mathbf{T}^{*}_{8}(2,3) = &-\cos(\mathbf{r}_2)\cdot\sin(\mathbf{r}_3)\cdot\sin(\mathbf{r}_5)\\ &+(-\cos(\mathbf{r}_2)\cdot\cos(\mathbf{r}_3)\cdot\sin(\mathbf{r}_4)\\ &-\sin(\mathbf{r}_2)\cdot\cos(\mathbf{r}_4))\cdot\cos(\mathbf{r}_5)\end{aligned}$$

$$^{D}\mathbf{T}^{*}_{p}(2,4) = \mathbf{d}_y$$

$$\begin{aligned}^{1}\mathbf{T}^{*}_{8}(2,4) = &(-\cos(\mathbf{r}_2)\cdot\sin(\mathbf{r}_3)\cdot\sin(\mathbf{r}_5)\\ &+(-\cos(\mathbf{r}_2)\cdot\cos(\mathbf{r}_3)\cdot\sin(\mathbf{r}_4)\\ &-\sin(\mathbf{r}_2)\cdot\cos(\mathbf{r}_4)\cdot\cos(\mathbf{r}_5))\cdot(\lambda_6+\mathbf{t}_p)\\ &-\lambda_5\cdot\cos(\mathbf{r}_2)\cdot\cos(\mathbf{r}_3)\cdot\sin(\mathbf{r}_4)\\ &-\lambda_5\cdot\sin(\mathbf{r}_2)\cdot\cos(\mathbf{r}_4)\\ &-(\lambda_3+\lambda_4)\cdot\sin(\mathbf{r}_2)\end{aligned}$$

$$^{D}\mathbf{T}^{*}_{p}(3,3) = -\cos(\theta_x)\cdot\cos(\theta_y)$$

$$\begin{aligned}^{1}\mathbf{T}^{*}_{8}(3,3) = &-(\sin(\mathbf{r}_1)\cdot\cos(\mathbf{r}_3)\\ &+\cos(\mathbf{r}_1)\cdot\sin(\mathbf{r}_2)\cdot\sin(\mathbf{r}_3))\cdot\sin(\mathbf{r}_5)\\ &+(-(-\sin(\mathbf{r}_1)\cdot\sin(\mathbf{r}_3)\\ &+\cos(\mathbf{r}_1)\cdot\sin(\mathbf{r}_2)\cdot\cos(\mathbf{r}_3))\cdot\sin(\mathbf{r}_4)\\ &+\cos(\mathbf{r}_1)\cdot\cos(\mathbf{r}_2)\cdot\cos(\mathbf{r}_4))\cdot\cos(\mathbf{r}_5)\end{aligned}$$

$$^{D}\mathbf{T}^{*}_{p}(3,4) = \mathbf{d}_z$$

$$\begin{aligned}^{1}\mathbf{T}^{*}_{8}(3,4) = &\lambda_1+(-(\sin(\mathbf{r}_1)\cdot\cos(\mathbf{r}_3)\\ &+\cos(\mathbf{r}_1)\cdot\sin(\mathbf{r}_2)\cdot\sin(\mathbf{r}_3))\cdot\sin(\mathbf{r}_5)\\ &+(-(-\sin(\mathbf{r}_1)\cdot\sin(\mathbf{r}_3)\\ &+\cos(\mathbf{r}_1)\cdot\sin(\mathbf{r}_2)\cdot\cos(\mathbf{r}_3))\cdot\sin(\mathbf{r}_4)\\ &+\cos(\mathbf{r}_1)\cdot\cos(\mathbf{r}_2)\cdot\cos(\mathbf{r}_4))\cdot\cos(\mathbf{r}_5))\cdot(\lambda_6+\mathbf{t}_p)\\ &-\lambda_5\cdot(-\sin(\mathbf{r}_1)\cdot\sin(\mathbf{r}_3)\\ &+\cos(\mathbf{r}_1)\cdot\sin(\mathbf{r}_2)\cdot\cos(\mathbf{r}_3))\cdot\sin(\mathbf{r}_4)\\ &+\lambda_5\cdot\cos(\mathbf{r}_1)\cdot\cos(\mathbf{r}_2)\cdot\cos(\mathbf{r}_4)\\ &+(\lambda_3+\lambda_4)\cdot\cos(\mathbf{r}_1)\cdot\cos(\mathbf{r}_2)\\ &+\lambda_2\cdot\cos(\mathbf{r}_1)+\mathbf{t}_d\end{aligned}$$

where θ_x, θ_y, θ_z, $\mathbf{d}_x$, $\mathbf{d}_y$, $\mathbf{d}_z$ are deformity parameters; $\mathbf{r}_1$, $\mathbf{r}_2$, $\mathbf{r}_3$, $\mathbf{r}_4$, $\mathbf{r}_5$, $\mathbf{t}_d$, $\mathbf{t}_p$ are pair variables; and λ_1, λ_2, λ_3, λ_4, λ_5, λ_6 are dimensional parameters in the fixator links.

$\lambda_1 = 17\,\text{mm}$, $\lambda_2 = 25\,\text{mm}$, $\lambda_3 = 15\,\text{mm}$, $\lambda_4 = 31\,\text{mm}$, $\lambda_5 = 25\,\text{mm}$, $\lambda_6 = 17\,\text{mm}$.

A.2. Orthofix

$$^{D}\mathbf{T}^{*}_{p}(1,1) = \cos(\theta_y)\cdot\cos(\theta_z)$$

$$\begin{aligned}^{1}\mathbf{T}^{*}_{4}(1,1) = &(-\cos(\beta_1)\cdot\sin(\gamma_1)\cdot\cos(\alpha_2)\\ &+\sin(\beta_1)\cdot\sin(\alpha_2))\cdot\sin(\gamma_2)\\ &-(-\cos(\beta_1)\cdot\cos(\gamma_1)\cdot\cos(\beta_2)\\ &+(\cos(\beta_1)\cdot\sin(\gamma_1)\cdot\sin(\alpha_2)\\ &+\sin(\beta_1)\cdot\cos(\alpha_2))\cdot\sin(\beta_2))\cdot\cos(\gamma_2)\end{aligned}$$

$$^{D}\mathbf{T}^{*}_{p}(1,2) = -\cos(\theta_y)\cdot\sin(\theta_z)$$

$$\begin{aligned}^{1}\mathbf{T}^{*}_{4}(1,2) = &(-\cos(\beta_1)\cdot\sin(\gamma_1)\cdot\cos(\alpha_2)\\ &+\sin(\beta_1)\cdot\sin(\alpha_2))\cdot\cos(\gamma_2)\\ &+(-\cos(\beta_1)\cdot\cos(\gamma_1)\cdot\cos(\beta_2)\\ &+(\cos(\beta_1)\cdot\sin(\gamma_1)\cdot\sin(\alpha_2)\\ &+\sin(\beta_1)\cdot\cos(\alpha_2))\cdot\sin(\beta_2))\cdot\sin(\gamma_2)\end{aligned}$$

$$^{D}\mathbf{T}^{*}_{p}(1,3) = \sin(\theta_y)$$

$$\begin{aligned}^{1}\mathbf{T}^{*}_{4}(1,3) = &\cos(\beta_1)\cdot\cos(\gamma_1)\cdot\sin(\beta_2)\\ &+(\cos(\beta_1)\cdot\sin(\gamma_1)\cdot\sin(\alpha_2)\\ &+\sin(\beta_1)\cdot\cos(\alpha_2))\cdot\cos(\beta_2)\end{aligned}$$

$$^{D}\mathbf{T}^{*}_{p}(1,4) = \mathbf{d}_x$$

$$^{1}\mathbf{T}^{*}_{4}(1,4) = \sin(\beta_1)\cdot(\mathbf{t}_0+\mathbf{s}_1+\mathbf{s}_2)$$

$$^{D}\mathbf{T}^{*}_{p}(2,3) = -\sin(\theta_x)\cdot\cos(\theta_y)$$

$$\begin{aligned}^{1}\mathbf{T}^{*}_{4}(2,3) = &(\cos(\alpha_1)\cdot\sin(\gamma_1)\\ &+\sin(\alpha1)\cdot\sin(\beta_1)\cdot\cos(\gamma_1))\cdot\sin(\beta_2)\\ &+(-(\cos(\alpha1)\cdot\cos(\gamma_1)\\ &-\sin(\alpha_1)\cdot\sin(\beta_1)\cdot\sin(\gamma_1))\cdot\sin(\alpha_2)\\ &-\sin(\alpha_1)\cdot\cos(\beta_1)\cdot\cos(\alpha_2))\cdot\cos(\beta_2)\end{aligned}$$

$$^{D}\mathbf{T}^{*}_{p}(2,4) = \mathbf{d}_y$$

$$^{1}\mathbf{T}^{*}_{4}(2,4) = -\sin(\alpha_1)\cdot\cos(\beta_1)\cdot(\mathbf{t}_0+\mathbf{s}_1+\mathbf{s}_2)$$

$$^{D}\mathbf{T}^{*}_{p}(3,3) = -\cos(\theta_x)\cdot\cos(\theta_y)$$

$$\begin{aligned}^{1}\mathbf{T}^{*}_{4}(3,3) = &(\sin(\alpha_1)\cdot\sin(\gamma_1)\\ &-\cos(\alpha_1)\cdot\sin(\beta_1)\cdot\cos(\gamma_1))\cdot\sin(\beta_2)\\ &+(-(\sin(\alpha_1)\cdot\cos(\gamma_1)\\ &+\cos(\alpha_1)\cdot\sin(\beta_1)\cdot\sin(\gamma_1))\cdot\sin(\alpha_2)\\ &+\cos(\alpha_1)\cdot\cos(\beta_1)\cdot\cos(\alpha_2))\cdot\cos(\beta_2)\end{aligned}$$

$$^{D}\mathbf{T}^{*}_{p}(3,4) = \mathbf{d}_z$$

$$^{1}\mathbf{T}^{*}_{4}(3,4) = \cos(\alpha_1)\cdot\cos(\beta_1)\cdot(\mathbf{t}_0+\mathbf{s}_1+\mathbf{s}_2)$$

where θ_x, θ_y, θ_z, $\mathbf{d}_x$, $\mathbf{d}_y$, and $\mathbf{d}_z$ are deformity parameters; α_1, β_1, γ_1, α_2, β_2, γ_2 and $\mathbf{t}_0$ are pair variables; and $\mathbf{s}_1$ and $\mathbf{s}_2$ are geometric design parameters in the central body.

$\mathbf{s}_1 = 30\,\text{mm}$, $\mathbf{s}_2 = 90\,\text{mm}$.

References

Chao, E.Y., Hein, T.J., 1988. Mechanical performance of the standard orthofix® external fixator. Orthopedics 11, 1057–1069.

Chao, E.Y.S., Morrey, B.F., 1978. Three-dimensional rotation of the elbow. Journal of Biomechanics 11, 57–73.

Chao, E.Y.S., Rim, K., Smidt, G.L., Johnston, R.C., 1970. The application of 4×4 matrix method to the correction of the

measurements of hip joint rotations. Journal of Biomechanics 3, 459–471.

Chao, E.Y.S., An, K.N., Askew, L.J., Morrey, B.F., 1980. Electrogoniometer for the measurement of human elbow joint rotation. Journal of Biomechanical Engineering 102 (4), 301–310.

Chao, E.Y.S., Neluheni, E.V.D., Hsu, R.W.W., Paley, D., 1994. Biomechanics of malalignment. Orthopaedic Clinics of North America 25 (3), 379–386.

Cooke, T.D., Pichora, D., Siu, D., Scudamore, R.A., Bryand, J.T., 1989. Surgical implications of varus deformity of the knee with obliquity of joint surfaces. Journal of Bone and Joint Surgery 71(4)-B, 560–565.

Egger, E.L., Gottsauner-Wolf, F., Palmer, J., Aro, H.T., Chao, E.Y., 1993. Effects of axial dynamization on bone healing. Journal of Trauma 34 (2), 185–192.

Goodship, A.E., Kenwright, J., 1985. The influence of induced micromovement upon the healing of experimental tibial fractures. Journal of Bone and Joint Surgery 67(4)-B, 650–655.

Grood, E.S., Suntay, W.J., 1981. Justification of triaxial goniometer for the measurement of joint rotation. Journal of Biomechanics 14 (9), 653–654.

Heijens, E., Gladbach, B., Pfeil, J., 1999. Definition, quantification, and correction of translation deformities using long leg, frontal plane radiography. Journal of Pediatric Orthopaedics B 8, 285–291.

Hsu, R.W.W., Himeno, S., Coventry, M.B., Chao, E.Y.S., 1990. Normal axial alignment of the lower extremities and load-bearing distribution at the knee. Clinical Orthopaedics and Related Research 255, 215–227.

Kanel, J.S., Price, C.T., 1995. Unilateral external fixation for corrective osteotomies in patients with hypophosphatemic rickets. Journal of Pediatric Orthopaedics 15 (2), 232–235.

Matsushita, T., Nakamura, K., Okazaki, H., Kurokawa, T., 1998. A simple technique for correction of complicated tibial deformity including rotational deformity. Archive of Orthopaedic Trauma Surgery 117 (4–5), 259–261.

McCarthy, J.M., 1986. Kinematics of Robotic Manipulators. MIT Press, Cambridge, MA.

Nikravesh, P.E., 1988. Computer-Aided Analysis of Mechanical System. Prentice-Hall, New Jersey.

Paley, D., Tetsworth, K., 1992. Mechanical axis deviation of the lower limbs: preoperative planning of uniapical deformities of the tibia and femur. Clinical Orthopaedics and Related Research 280, 48–64.

Paley, D., Chaudray, M., Pirone, A.M., Lentz, P., Kautz, D., 1990. Treatment of malunions and mal-nonunions of the femur and tibia by detailed preoperative planning and the ilizarov techniques. Orthopaedic Clinics of North America 21 (4), 667–691.

Shigley, J.E., 1969. Kinematic Analysis of Mechanisms, 2nd ed. McGraw-Hill, New York.

Wolf, S., Augat, P., Eckert-Hubner, K., Laule, A., Krischak, G.D., Claes, L.E., 2001. Effects of high-frequency, low-magnitude mechanical stimulus on bone healing. Clinical Orthopaedics and Related Research 385, 192–198.

Appendix 4

1: Anticancer Res 2002 Jul-Aug;22(4):1971-5

The effect of a doxorubicin, cisplatin and ifosfamide combination chemotherapy on bone turnover.

Virolainen P, Inoue N, Nagao M, Frassica FJ, Chao EY.

Department of Orthopaedic Surgery, The Johns Hopkins University, Baltimore, Maryland 21205-2196, USA.

BACKGROUND: Use of combination adjuvant chemotherapies have improved the disease-free survival rate of tumor patients significantly. Previous experimental studies have shown that chemotherapeutic agents have negative effects on fixation of porous coated prosthesis, but the effects on normal bone turnover rate and mechanicalproperties have been reported to be minimal. MATERIALS AND METHODS: Fourteen dogs were used to study the effect of a doxorubicin, cisplatin and ifosfamide combination in normal bone turnover. We developed a safe and clinically-relevant canine model for multidrug perioperative chemotherapy that simulates current cancer treatment. The bone specimens were analyzed using microradiography, bone histomorphometry and torsional testing. The results were compared with canines that underwent a similar surgical protocol without chemotherapy. RESULTS: The results showed no differences in mechanical properties after 22 weeks of chemotherapy. The porosity, osteonal activity and mineral apposition rate of the cortical bone were unaffected. The results also showed no difference in porosity of perimeter in cancellous bone, but the mineral apposition rate was significantly reduced. CONCLUSION: The difference in mineral appostion rate of cancellous bone shows that, although the effect of temporary chemotherapy on bone may have minor effects on normal turnover and that the effect may be reversible, it causes disturbance in bone mass accumulation. This may later raise the risk for fragility fractures and osteoporosis.

PMID: 12174872 [PubMed - in process]

Appendix 5

TRABECULAR MICROSTRUCTURE IN THE EARLY STAGE OF CORTICAL DEFECT REPAIR

*Rafiee, B; *Inoue, N (A-Department of The Army); *Jones, K; *Deitz, L; *Aro, H; +*Chao, E
+*Orthopaedic Biomechanics Laboratory, Johns Hopkins University, Baltimore, Maryland. Ross Research Building, 720 Rutland Avenue, Room 235, Baltimore, MD 21205, 410-502-6416, Fax: 410-502-6414, eychao@eagle.gsh.jhu.edu

INTRODUCTION: Cortical bone defect repair contrasts fracture and osteotomy healing by its stable mechanical condition. Lacking a cartilaginous phase, it follows an intramembranous ossification[1] specifically termed "angiogenic ossification" by Krompecher[2]. The limited available studies on cortical defect repair have used small circular defects[1] which fail to create a sufficient stress-strain gradient to fully characterize the influence of mechanical loading on the repair process. This study quantitatively analyzed trabecular orientation in a rectangular, high stress-strain gradient, cortical defect during its early stage of repair.

METHODS: Rectangular bone defects of dimensions 0.25 OD (the outer diameter of the tibia) by 1.5 OD (approximately, 2.5x15 mm) were created in the mid-diaphysis of the medial cortex of the right tibia in seven beagles by drilling 2.4 mm holes and connecting them with a fine osteotome. Dogs were euthanized after 4 weeks of unrestricted weight bearing. The proximal half of the defect was cut into six 1 mm thick transverse sections, processed undecalcified, and embedded in MMA (Fig. 1). The 2nd, 4th, and 6th sections were ground to 100 μm. The 1st, 3rd, and 5th transverse sections were each further cut longitudinally in the medial tibial plane, parallel to the defect surface, to form four 100 μm thick longitudinal sections, three from the defect area and one from anterior portion of the medullary canal (Fig. 1). Contact microradiographs of the transverse and longitudinal sections were made and digitized under 50x light microscopy for 2-dimensional Fast Fourier Transform (FFT) analysis. Transverse section images were divided into 9 fields in the defect area and 15 in the medullary canal (Fig. 3). Longitudinal sections of the defect area and medullary canal were divided into 3 and 5 fields, respectively. Each field corresponded to a 0.85 mm x 0.85 mm area in the radiograph and a 256x256 pixel array in the digitized image. FFT yielded a quantified orientation angle and intensity for each field (Fig. 2D-F). Statistical significance of the variance in angle and intensity of orientations in the above mentioned fields was demonstrated by ANOVA with corroborating post-hoc t-tests.

RESULTS: No clear bone formation was observed from the periosteal surface. Generally, repair bone trabeculae oriented from the medullary canal towards the bone defect. The intensity of trabecular orientation was higher in the defect area than in the medullary canal ($p<0.01$). These intradefect trabeculae oriented parallel to the defect walls. The vectorial mean angles of trabecular orientation in the fields chosen in the edge transverse sections had statistically significant differences from those in the center section ($p<0.05$). Analysis of the longitudinal sections quantified that trabeculae in the middle of the defect, on the outermost surface, were oriented along the longitudinal axis of the bone, but this orientation changed to a transverse direction in the deeper layers. In the longitudinal sections, the first two layers of the center field demonstrated statistically significant differences in the angle of orientation from fields to either side and in deeper layers ($p< 0.05$).

DISCUSSION: Early in the repair phase of a round cortical defect in rabbits, Shapiro proposed a rich vascular ingrowth from the medullary canal towards the defect, perpendicular to the cortical haversian systems, followed by woven bone and trabecular formation parallel to this vascular pattern[1]. Suwa used the microvascular casting method to analyze microvascular and trabecular changes in defect repair and demonstrated similar results[3]. Highly oriented trabecular structure in the defect area may reflect the structure of early vascular networks. Redirection of trabecular structure towards the osteonal direction was not observed by Shapiro's model even 12 weeks after surgery. In the current study, trabecular orientation in the osteonal direction was observed in a limited area. This may be caused by a higher stress-strain gradient around the bone defect[4]. Some trabecular orientation initiated from the endosteal surface adjacent to the defect towards the defect was observed in transverse section 6, from near the edge of the defect. It may be related to the higher stress-strain gradient in the corresponding area. Recent studies indicate the presence of growth factors and cytokines which may induce angiogenesis within the cortex and molecular transport through load-induced fluid flow[5-8]. Further study will be required to elucidate the contribution of the existing cortical bone to the defect healing process.

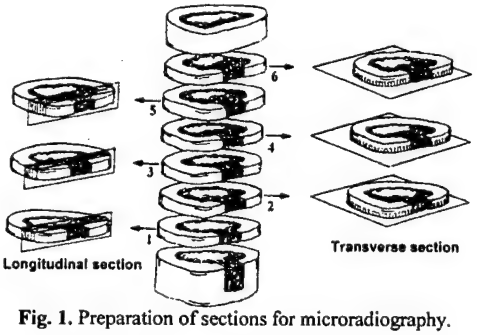

Fig. 1. Preparation of sections for microradiography.

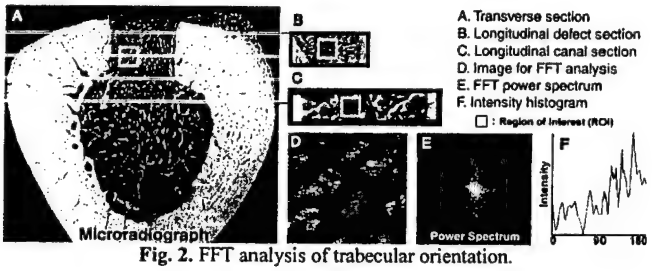

Fig. 2. FFT analysis of trabecular orientation.

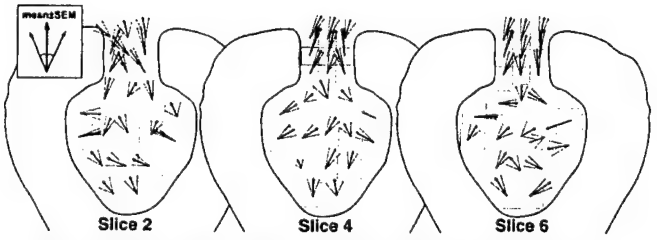

Fig. 3. Results of mean angle and intensity of the trabecular orientation.

REFERENCES: 1)Shapiro F:JBJS 70A,1067-81,1988. 2)Krompecher S: Verhand Anat Gesellshaft 42,34-53,1934. 3)Suwa F et al:J Osaka Dent Univ 32, 27-34,1998. 4)Elias J et al: Trans ORS23,973,1998. 5)Dekel S et al: JBJS 63B,185-9,1981. 6)Harada S et al:CORR313,76-80,1995. 7)Murry D & Rushton N:Calcif Tissue Int47,35-9,1990. 8)Knothe Tate M et al:Bone 22, 107-17,1998.

Appendix 6

BED-Vol. 50, 2001 Bioengineering Conference
ASME 2001

STUDY ON EXTERNAL FIXATOR ADJUSTABILITY USING SIMULATION AND VISUALIZATION MODEL

Yoon Hyuk Kim, John J. Elias, Nozomu Inoue and Edmund Y.S. Chao

Orthopaedic Biomechanics Laboratory
Johns Hopkins University
Baltimore, Maryland

INTRODUCTION

An external fixator is commonly used to stabilize fractured long bone segments. After inserting the pins and applying the fixator, adjustment of the position of each fragment is often necessary to reduce the fracture site and correct any residual deformities. A primary goal of external fixator design is allowing adequate adjustability for fracture reduction. The combination of an external fixator and a fractured bone can be modeled as a multi-link kinematic mechanism. Using computational techniques, the translations and rotations in the connecting joints of the mechanism necessary to reduce a given fracture can be rapidly quantified. Applying the calculated translations and rotations to a virtual biomechanical model of the fixator and bone system allows 3-D visualization of the adjustments required to reduce a fracture. The objective of this paper is to present a computational and graphical model of an external fixator that can be used to evaluate the fixator design, optimize the design, and guide clinicians using the device.

METHODS

The simulation model was based on an Orthofix, D.A.F external fixator. The model includes the mathematical representation of the motion of each link of the fixator and the bone segments as a kinematic linkage connected by various joints (Fig. 1). The distal bone fragment (D) was fixed to the origin of the global coordinate system (G), with the primary axes of the bone aligned with the global axes. The position of the proximal bone (P) within the global coordinate system was described using a 4 × 4 homogeneous transformation matrix, ${}^{G}\mathbf{T}_{P}$, which can be determined radiographically using established bone landmarks [1, 2]. This matrix is equivalent to the transformation of each link of the fixator from the proximal bone segment to the distal bone within the global coordinate system, as:

$$ {}^{G}\mathbf{T}_{P} = {}^{G}\mathbf{T}_{D} \cdot {}^{D}\mathbf{T}_{1} \cdot {}^{1}\mathbf{T}_{2} \cdot {}^{2}\mathbf{T}_{3} \cdot {}^{3}\mathbf{T}_{4} \cdot {}^{4}\mathbf{T}_{P}, \qquad (1), $$

where ${}^{G}\mathbf{T}_{D}$ is a 4 × 4 unit matrix representing the position of the distal bone in the global coordinate system, and the other transformations represent transformation of each segment of the linkage (Fig. 1). ${}^{D}\mathbf{T}_{1}$ and ${}^{4}\mathbf{T}_{P}$ represent rigid body translations in the directions of the pins. For the current model, the pin length was set to 40 mm. In addition, ${}^{2}\mathbf{T}_{3}$ represents a rigid body translation along the length of the telescoping slider mechanism within the body of the fixator. Also, ${}^{3}\mathbf{T}_{4}$ and ${}^{1}\mathbf{T}_{2}$ are pure rotations at the ball and socket joints. The rotation sequence of the ball and socket joints for α_i, β_i, and γ_i, i=1 and 2, is Rot(x)-Rot(y`)-Rot(z``), as a standard Briant angle convention[3]. The maximum allowable length of the translation for the telescoping slider and the rotation angle for the ball and socket joints are 40 mm and 20°, respectively. The initial malalignment is expressed within ${}^{G}\mathbf{T}_{P}$ as rotations around the axes of the fragment and a translation along the long axis of the bone. To realign the bones, the resulting system of equations is solved for the rotation or translation at each joint. For this model the length of the bone from the fracture site to the closest pin on both the proximal and distal segments was set to 80 mm.

After substituting in the known values in the transformation matrices, ${}^{G}\mathbf{T}_{D}$, ${}^{D}\mathbf{T}_{1}$ and ${}^{4}\mathbf{T}_{P}$, Eq. 1 can be reduced as follows:

$$ {}^{1}\mathbf{T}_{4} = {}^{1}\mathbf{T}_{2} \cdot {}^{2}\mathbf{T}_{3} \cdot {}^{3}\mathbf{T}_{4}, \qquad (2), $$

where

$$ {}^{1}\mathbf{T}_{4}(1,4) = \mathrm{Cos}(\beta_1) * t_2, $$

$$ {}^{1}\mathbf{T}_{4}(2,4) = -\mathrm{Sin}(\alpha_1) * \mathrm{Cos}(\beta_1) * t_2, $$

$$ {}^{1}\mathbf{T}_{4}(3,4) = \mathrm{Cos}(\alpha_1) * \mathrm{Cos}(\beta_1) * t_2, $$

where α_1, β_1 and t_2 are two angle parameters in ${}^{1}\mathbf{T}_{2}$ and the translation parameter in ${}^{2}\mathbf{T}_{3}$, respectively (Fig. 1). After solving for t_2, α_1 and β_1 using the three equations in Eq. (2) and calculating γ_1 using the projection method, α_2, β_2, and γ_2 are solved using three other equations in Eq. (2). Two clinical cases, a rotational malalignment combined with a fracture gap between two bone segments and a varus angulation, were investigated to validate the model and the analysis involved.

RESULTS

In the first case, a rotational malalignment combined with a fracture gap between two bone segments is considered. The initial gap and the rotational malalignment were set to 6 mm and 30°, respectively. One possible solution is given in Fig. 2 for both the proximal and the distal ball joints as (α_1, β_1, γ_1)=(5°, -18°, 16°), (α_2, β_2, γ_2)=(-10°, -16°, 16°) and no extension in the slider (Fig. 2). In the second case, 10° varus angulational deformity correction is simulated and visualized (Fig. 3). The candidate solution to correct the deformity was estimated as (α_1, β_1, γ_1)=(5°, 0°, 0°), (α_2, β_2, γ_2)=(5°, 0°, 0°) and t_2 =12.3 mm. The graphical models clearly depict where the adjustments were performed to reduce the bone segment malalignment perfectly. It is important to realize that the component adjustments are sequence dependent according to the order of the transformation matrices multiplication assigned. The order of adjustment can be changed which may produce a different solution, thus making the adjustability of a fixator nonunique.

DISCUSSION

External fixators are often applied to polytrauma cases under an environment in which adequate imaging equipment may not be available to provide acceptable fracture segment reduction. Therefore, subsequent adjustment of the fracture ends is often required for a more complex device. Unfortunately, this issue of design requirement rarely has been investigated and this study provides a systematic approach to this problem. Using the kinematic linkage model, the rotational malalignment combined with a fracture gap displacement could be modeled and analyzed. Although the adjustment solution may not be unique, the model quantified the order and the magnitude of translation and rotation for each joint of the fixator to align the bone ends. These calculated adjustments could reduce the fracture malalignment and angulation, but they may not be feasible due to bone fragments collision or to produce excessive soft tissue stretching during reduction. Visualization of the sequential adjustments used to reduce the fracture gap based on alternative solutions should help to determine the clinical feasibility of the reduction process. Further development of the model should include constraints to avoid collision or excessive soft tissue extension. These graphical model and analysis simulation are powerful tools to evaluate and validate the device performance.

The simulation model allows the kinematic analysis results to be visualized. The bone and pin length, and the initial deformity are input to the model. This model and analysis technique can be used to illustrate the necessary fixator component adjustment to correct the malalignment, making the system a valuable preoperative planning tool and a teaching aid. This simulation technology is now being extended to study the strength and stiffness of the fixator under physiological loading. Stress/strain analyses can also be incorporated in the future to reduce the need for mechanical testing of these devices. By incorporating the translational or rotational limit of each joint, the model can also be used to determine the limits of adjustability inherent to a given fixator design.

REFERENCES

1. Chao, E.Y.S., Rim, K., Smidt, G.L. and Johnston, R.C., 1970, "The Application of 4 X 4 Matrix Method to the Correction of the Measurements of Hip Joint Rotations," J. Biomech., Vol. 3, pp. 459-471.
2. McCarthy J.M., 1986, *Kinematics of Robotic Manipulators*, MIT Press.
3. Nikravesh P.E., 1988, *Computer-Aided Analysis of Mech. Sys.*, Prentice Hall.

ACKNOWLEDGEMENT

This study was supported in part by U.S. Army Medical Research and Material Command(USAMRMC) and a gift from EBI Biomedical System Inc.

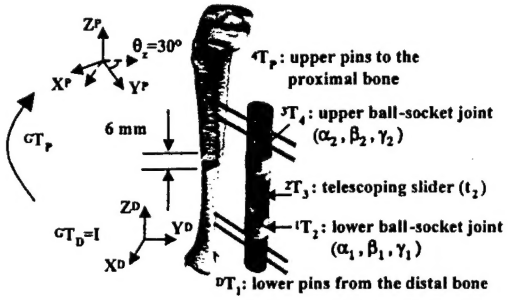

Figure 1. A bone and fixator system with rotational malalignment combined with a fracture gap.

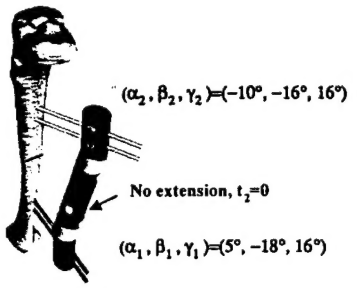

Figure 2. A bone and fixator system after correction.

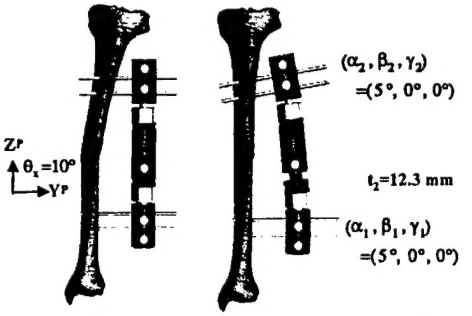

Figure 3 A bone and fixator system in a 10° varus angular deformity correction.

Appendix 7

Application of virtual interactive musculoskeletal system to bone deformity correction using unilateral external fixator

Y.H. Kim, J.J. Elias, N. Inoue, E.Y.S. Chao

Orthopaedic Biomechanics Laboratory, Johns Hopkins University, Baltimore, MD 21205-2196, USA

1. Introduction

This paper presents a virtual interactive musculoskeletal system (VIMS) software of an external fixator used to quantify the fixator adjustability and the correction of bone deformity. This software offers the graphic models, the biomechanical analysis algorithms and the virtual laboratory environment to evaluate fixator design and guide clinicians using the device as a pre-operative planning tool.

2. Methods

The fixator model is composed of four pins connected to the bone, two telescoping pin clamps connecting to the bone, a central rotary joint and four sets of hinge joints. The model includes the mathematical representation of the motion of the fixator and the bone segments as a kinematic linkage connected by various joints (Fig. 1). The distal bone fragment (D) was fixed to the origin of the global coordinate system. The relative position and orientation of the proximal tibial bone (P) with respect to the distal tibial segment (D) was expressed by a 4×4 homogeneous transformation matrix, ${}^{D}T_{P}$. This matrix is equivalent to the transformation of each link of the fixator from the proximal system to the distal bone system by the matrix equation:

$$ {}^{D}T_{P} = {}^{D}T_{1} \cdot {}^{1}T_{2} \cdot {}^{2}T_{3} \cdot {}^{3}T_{4} \cdot {}^{4}T_{5} \cdot {}^{5}T_{6} \cdot {}^{6}T_{7} \cdot {}^{7}T_{8} \cdot {}^{8}T_{P}. \quad (1) $$

${}^{D}T_{1}$ and ${}^{8}T_{P}$ represent rigid body translations of the pins along the clamp pin slots. ${}^{1}T_{2}$ and ${}^{7}T_{8}$ represent rigid body translations along the length of the telescoping slider mechanism within the body of the clamps. Also, ${}^{2}T_{3}$, ${}^{3}T_{4}$, ${}^{4}T_{5}$, ${}^{5}T_{6}$ and ${}^{6}T_{7}$ are the rotations at the revolute joints. To correct the bone malalignment, the system of equations is solved for the rotation or translation at each joint following a pre-determined sequence of adjustment. After substituting in an assumed pin length in the transformation matrices and applying an arbitrary equality constraint, $t_d = t_p$, six independent nonlinear equations can be solved for six unknown joint variables using the modified Newton's method. A graphic-based solid model of a tibia was developed using the 3D reconstruction of CT Scan data. The graphic model of the fixator was developed using CAD software to easily visualize the analysis results.

A rotational malalignment of 30° with a fracture gap of 10mm was used as a test example to validate the analytical formulation and graphically demonstrate fracture reduction.

3. Results

The calculated joint variable values were $r_1 = 14.73°$, $r_2 = 44.06°$, $r_3 = 41.88°$, $r_4 = 42.28°$, and $r_5 = 14.88°$. The translations at the two telescoping clamps, t_d and t_p, were 1.43mm for both joints. The graphic model showed that the bone fragments were perfectly aligned following reduction. However, the pathways capable of reaching the final correction are infinite. Optimal solution was found by minimizing soft callus disruption with no bone ends collision.

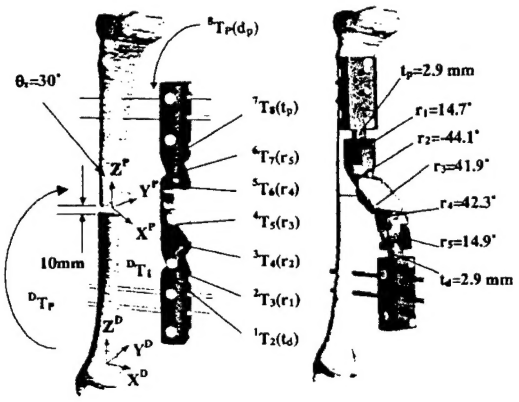

Fig. 1. The bone–fixator system in 30 rotational deformities with 10mm fracture gap.

4. Discussion and conclusions

The component adjustments are sequence dependent according to the order of the transformation matrices multiplication. The VIMS software allows the kinematic analysis results to be visualized. These models and biomechanical analysis techniques can be used to study fixator component adjustments needed to align bone fragments, making the system a valuable preoperative planning tool and a teaching aid.

Acknowledgements

Supported by US Army Med. Res. & Material Command, Bristol Myers Center of Excellence Award & an EBI gift.

References

[1]Chao EYS, et al. (1970). J. Biomech 3:459–71.

Standing equilibrium after a running stress test

M. Kuczynski[a], D. Nawarecki[b]

[a] *Department of Rehabilitation Sciences, Polytechnic University, Hong Kong*
[b] *Department of Physical Therapy, Technical University in Opole, Opole, Poland*

1. Introduction

Stability of human equilibrium system is influenced by several factors. In particular, fatigue may cause substantial increase in body sway that can affect the performance in different sport activities. Recently, it has been established that fatigue produced by bicycle riding led to significant changes in postural stability. The question arises what are the possible reasons of a surge in postural sway

Appendix 8

It should be mentioned, that the fibrils are not added as a separate material, in fact the structure is created during MFC manufacturing.

3. Results

Fig. 1 indicates the feasibility of manufacturing this new biodegradable fibrillar reinforced composite. First, after blending an isotropic structure with separately arranged phases of both components can be observed. After the final stage of MFC-treatment this structure can be changed into a fibrillar structure. The resorbable composites produced by the MFC technique showed high strength and high modulus, shown in Table 1. The bending strength can be increased nearly twice and the bending stiffness is about 80% higher in comparison to the nonreinforced pin. The produced rods can be simply processed into more complex shapes such as surface structured, bone fixation implant nails.

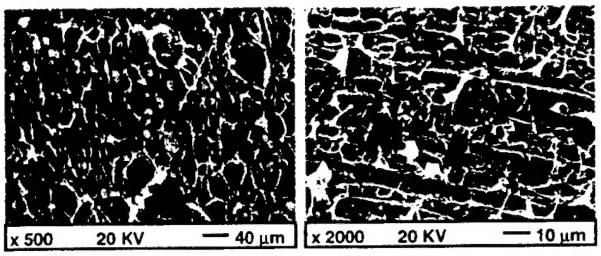

Fig. 1. SEM-micrographs of the split surface after different processing steps: after blending (left) and after annealing (right).

Table 1
Mechanical properties of the different bone nails

	Bending strength (%)	Bending stiffness (%)
Nonreinforced-nail	100	100
MFC-nail	190	180

4. Discussion and conclusions

Regarding the mechanical properties, a new promising biodegradable polymeric composite is provided. For the future work the degradation behavior of this composite will be analyzed.

Acknowledgements

The authors acknowledge the financial support of the foundation of Rhineland-Palatinate for Innovation and the material support of Boehringer Ingelheim KG (Ingelheim, Germany).

References

[1]Wintermantel E (1996). Biokompatible Werkstoffe und Bauweisen. Berlin: Springer.
[2]Weiler W, Gogolewski S (1996). Biomaterials 17:529–35.
[3]Törmälä P (1992). Clin Mater 10:29–34.
[4]Fakirov S, Evstatiev M, Friedrich K (1998) Proceedings Polymerwerkstoffe 98: 125-33.

Vascular and trabecular microstructures in the early stage of cortical defect repair

N. Inoue[a], B. Rafiee[a], I. Toda[b], Y. Tamada[b], F. Suwa[b], H.T. Aro[a], E.Y.S. Chao[a]

[a]*Orthopaedic Biomechanics Laboratory, Johns Hopkins University, Baltimore, USA*
[b]*Department of Anatomy, Osaka Dental University, Osaka, Japan*

1. Introduction

Cortical bone defect repair follows intramembranous ossification[1]. Intra-membranous ossification is termed "angiogenic ossification" by Krompecher[2] and contribution of the initial vascular structure to the subsequent trabecular formation has been postulated[3]. This study analyzed micro-vascular and trabecular structures in a rectangular cortical defect during its early stage of repair.

2. Methods

Longitudinal rectangular cortical bone defects were created in the middiaphysis of the tibia in nine canines. The dogs were euthanized 1 week after surgery for microvascular analysis ($n=2$: defect size; 1.0×0.25 of outer diameter) and 4 weeks after surgery ($n=7$: defect size; 1.5×0.25 of outer diameter) for trabecular structure analysis. A plastic microcorrosion casting was used for the microvascular analysis[3]. The defect was cut in sagittal and transverse sections for microvascular analysis (Fig 1). For the trabecular analysis, contact microradiographs of transverse and coronal sections were analyzed using two dimensional fast Fourier transform (FFT) analysis (Fig. 2).

3. Results

Microvascular analysis revealed that the capillary in the defect were oriented from the medullary canal towards the bone defect. Capillary formation from the endosteal surface towards the defect was also observed (Fig. 1). In the trabecular structure analysis, the intradefect trabeculae were oriented perpendicular to the long axis of the tibia.

Fig. 1. Scanning electron micrographs of the vascular casts 1 week after surgery. Sagittal (left) and transverse (right) sections.

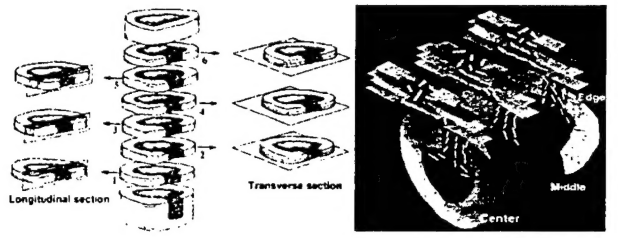

Fig. 2. Trabecular orientation 4 weeks after surgery quantified with FFT analysis.

The intensity of trabecular orientation was significantly higher in the defect area than in the medullary canal and also higher in the edge sections than the center sections. In the medullary canal, trabecular orientation was from the endosteal surface towards the defect. This orientation was more pronounced in the edge sections. In the longitudinal sections, trabecular orientation was predominantly transverse. However, longitudinal redirection was observed in the most superficial layer and at the corners of the defect (Fig 2).

4. Discussion and conclusions

The repair mechanism of cortical bone defect differs from that of fracture and osteotomy due to its stable mechanical condition and lack of micro-motion. Therefore, magnitude of the stress in hematoma or granulation tissue formed within the bone defect appears to be minimal until calcified tissue is formed within the defect, even though the rectangular bone defect creates high stress gradient in the cortex around the defect. In fact, orientation of the capillaries was perpendicular to the principal stress axis of the tissue. The overall orientation of the trabeculae formed 4 weeks after surgery coincided with the orientation of the capillary structures, indicating that capillary formation provides the initial structure of the trabecular formation. However, reorientation of the trabecular structure was observed at the corners of the defect, where a high strain energy density gradient was calculated by finite element analysis[4]. This remodeling of trabecular structures was not demonstrated in Shapiro's round-hole model even after 12 weeks[1]. Remodeling of the trabecular structures in the later phase is being studied using the same rectangular defect model to demonstrate the biomechanical factor on the remodeling.

Acknowledgements

Supported by AO Research Grant (2000-I18) and U.S. Army Medical Research and Material Command.

References

[1]Shapiro F (1988). JBJS 70A: 1067–81.
[2]Krompecher S (1934). Verhand Anat Gesellshaft 42: 34–53.
[3]Suwa F, et al. (1998). J Osaka Dent Univ 32: 27–34.
[4]Elias J, et al. (1998). Trans ORS 23: 973.

Usage of ultrasound for local bone injuries monitoring

Yu. Dekhtyar, I. Derjugina, J. Katasheva, A. Katashev, A. Tatarinov

Riga Technical University, Riga, Latvia

1. Introduction

Investigation of bone healing, stimulated by various physical agents (light, electromagnetic or ionizing radiation, etc.) requires methods to monitor bone injuries in vivo. Unfortunately, conventional methods, such as X-ray diagnostics or CT, are not suitable for such a purpose, because X-ray radiation may significantly interfere affection of the above physical factors affection. The main advantage of ultrasonic (US) methods to evaluate healing of bone is their non-invasiveness in a broad sense: diagnostic ultrasound is not just avoiding surgical procedures, but also would have a minor interference with healing process. Besides, there are a number of significant limitations and difficulties in the interpretation of the results, mainly due to complex interaction between US wave and overlaying soft tissues.

The present work estimates the usage of ultrasound to determine the size of local injuries in the rabbit lower jaw in vitro bearing in mind further extension of this technique to the in vivo measurements for injuries healing monitoring.

2. Methods

The injuries were modeled in vitro by splits of the various depths, made in various numbers on the lower edge of the jaw by dental split-disc (Fig. 1). Soft tissue coverage was modeled by slice of bovine tendon, smeared with ultrasonic gel and applied mechanically over the damaged jaw edge.

Effective velocity of ultrasound propagation across the injury was assessed both for open bone and bone, covered with soft tissue. To achieve this, measurements of US impulse propagation time was made, using US probe with constant base[1]. The effective velocity was calculated by dividing measurement base on propagation time.

3. Results

Due to difficulties in the assessment of the splits volume, surface covered by defect on the jaw side view was taken as a measure of the injury size. Effective US propagation velocity decreased with total

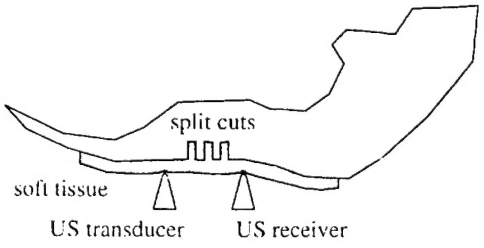

Fig. 1. Scheme of the experimental setup.